



CMYA5 is a novel interaction partner of FHL2 in cardiac myocytes

Konstantina Stathopoulou^{1,2} , Josef Schnittger^{1,2}, Janice Raabe^{1,2}, Frederic Fleischer^{1,2}, Nils Mangels³, Angelika Piasecki^{1,2}, Jane Findlay⁴, Kristin Hartmann⁵, Susanne Krasemann⁵, Saskia Schlossarek^{1,2}, June Uebeler^{1,2}, Viktor Wixler⁶, Derek J. Blake⁷, George S. Baillie⁴ , Lucie Carrier^{1,2}, Elisabeth Ehler^{8,9} and Friederike Cuello^{1,2}

1 Institute of Experimental Pharmacology and Toxicology, Cardiovascular Research Center, University Medical Center Hamburg-Eppendorf, Germany

2 DZHK (German Center for Cardiovascular Research), partner site Hamburg/Kiel/Lübeck, University Medical Center Hamburg-Eppendorf, Germany

3 Department of Biochemistry and Molecular Cell Biology, University Medical Center Hamburg-Eppendorf, Germany

4 Institute of Cardiovascular and Medical Sciences, University of Glasgow, UK

5 Institute of Neuropathology, University Medical Center Hamburg-Eppendorf, Germany

6 Institute of Molecular Virology, Centre for Molecular Biology of Inflammation, Westfaelische Wilhelms-University, Germany

7 Division of Psychological Medicine and Clinical Neurosciences, School of Medicine, Cardiff University, UK

8 School of Cardiovascular Medicine and Sciences, BHF Research Excellence Centre, King's College London, UK

9 Randall Centre for Cell and Molecular Biophysics (School of Basic and Medical Biosciences), King's College London, UK

Keywords

cardiac myocyte; cardiomyopathy-associated 5; four-and-a-half LIM domains protein 2; hypertrophy; scaffold protein; transcription

Correspondence

K. Stathopoulou and F. Cuello, Institute of Experimental Pharmacology and Toxicology, University Medical Center Hamburg-Eppendorf, Martinistrasse 52, Hamburg 20246, Germany
 Tel: +49 (0) 40/7410 57204
 E-mails: k.stathopoulou@uke.de (KS); f.cuello@uke.de (FC)

Konstantina Stathopoulou and Josef Schnittger joint first author

Konstantina Stathopoulou and Friederike Cuello joint corresponding author

Four-and-a-half LIM domains protein 2 (FHL2) is an anti-hypertrophic adaptor protein that regulates cardiac myocyte signalling and function. Herein, we identified cardiomyopathy-associated 5 (CMYA5) as a novel FHL2 interaction partner in cardiac myocytes. *In vitro* pull-down assays demonstrated interaction between FHL2 and the N- and C-terminal regions of CMYA5. The interaction was verified in adult cardiac myocytes by proximity ligation assays. Immunofluorescence and confocal microscopy demonstrated co-localisation in the same subcellular compartment. The binding interface between FHL2 and CMYA5 was mapped by peptide arrays. Exposure of neonatal rat ventricular myocytes to a CMYA5 peptide covering one of the FHL2 interaction sites led to an increase in cell area at baseline, but a blunted response to chronic phenylephrine treatment. In contrast to wild-type hearts, loss or reduced FHL2 expression in *Fhl2*-targeted knockout mouse hearts or in a humanised mouse model of hypertrophic cardiomyopathy led to redistribution of CMYA5 into the perinuclear and intercalated disc region. Taken together, our results indicate a direct interaction of the two adaptor proteins FHL2 and CMYA5 in

Abbreviations

5(6)-FAM, 5(6)-carboxyfluorescein; Aa, amino acids; AKAP, A-kinase-anchoring protein; ARVM, adult rat ventricular myocytes; BBC, B-box coiled coil; BSA, bovine serum albumin; CMYA5, cardiomyopathy-associated 5; CREB, cAMP-response element-binding protein; DAPI, 4', 6'-diamidin-2-phenylindol; ECL, enhanced chemiluminescence; ERK2, extracellular signal-regulated kinase 2; FCS, fetal calf serum; FHL2, four-and-a-half LIM domains protein 2; FMOC, fluorenylmethyloxycarbonyl; FNIII, fibronectin type III; GAPDH, glyceraldehyde-3-phosphate dehydrogenase; GST, glutathione-S-transferase; H&E, haematoxylin and eosin; HCM, hypertrophic cardiomyopathy; HRP, horseradish peroxidase; HS, horse serum; IP, immunoprecipitation; IPTG, isopropyl- β -thiogalactopyranoside; JPH2, junctophilin 2; KI, knock-in; KO, knockout; MEF2, myocyte enhancer factor 2; MM, maintenance medium; NRVM, neonatal rat ventricular myocytes; PBS, phosphate-buffered saline; PE, phenylephrine; PFA, paraformaldehyde; PKA, cAMP-dependent protein kinase; PLA, proximity ligation assay; PVDF, polyvinylidene fluoride; qPCR, quantitative PCR; RyR2, ryanodine receptor 2; S/N, supernatant; SPRY, SPL α and ryanodine receptor; TAC, transverse aortic constriction; TFA, trifluoroacetic acid; TIPS, triisopropylsilyl ether; TRIM, tripartite motif; WGA, wheat germ agglutinin; WT, wild-type.

cardiac myocytes, which might impact subcellular compartmentation of CMYA5.

(Received 23 June 2021, revised 13 January 2022, accepted 15 February 2022)

doi:10.1111/febs.16402

Introduction

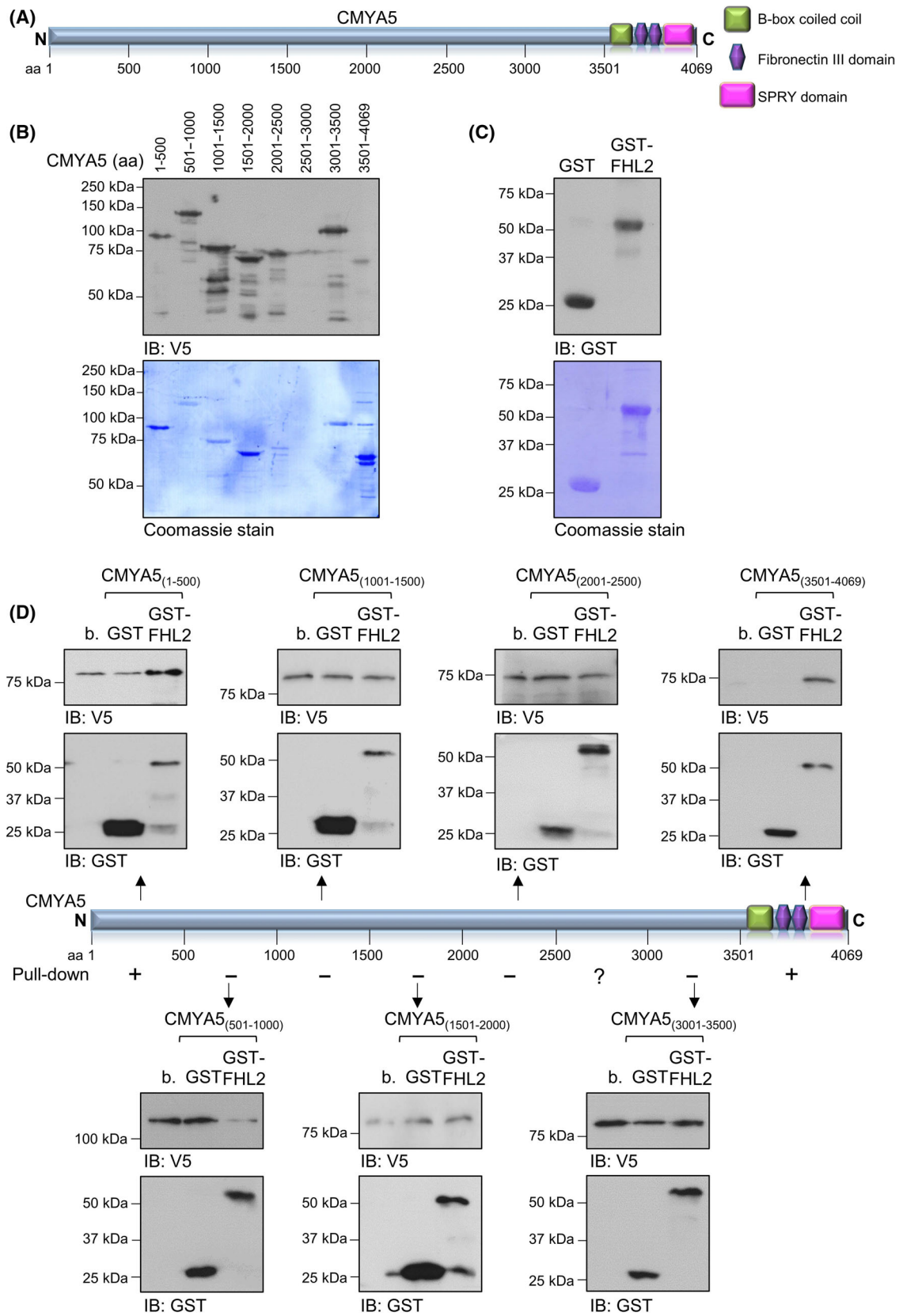
Cardiac myocyte and, subsequently, heart function are fine-tuned by signal transduction pathways that enable adaptation to changes in physiological demand. Deregulation of these pathways contributes to heart disease development. Therefore, identification and manipulation of proteins involved is of therapeutic interest. Scaffold and adaptor proteins play an important role in the spatio-temporal organisation of signal transduction pathways, tethering them to specific subcellular compartments [1].

Four-and-a-half LIM domains protein 2 (FHL2, also called DRAL) is such an adaptor protein in cardiac myocytes. As the name suggests, the main structural features of FHL2 are its LIM domains, which comprise each two zinc fingers and enable protein–protein interactions [2]. The FHL2 protein level was attenuated in different types of human heart failure [3–6] and in experimental models of heart disease [4,7]. The significance and potential functions of FHL2 in cardiac myocytes are illustrated by its various interaction partners. FHL2 interacts with proteins that include, among others, kinases, like the extracellular signal-regulated kinase 2 (ERK2) [8], protein kinase D1 [9] and sphingosine kinase 1 [10], the phosphatase calcineurin [11] and metabolic enzymes [12], which overall implicate FHL2 in the regulation of cardiac myocyte growth, cell survival and metabolism. Concerning

ERK2 and calcineurin, interaction with FHL2 has been shown to inhibit their pro-hypertrophic effects [8,11], indicating a protective role of FHL2 from cardiac hypertrophy. This hypothesis is supported by the observation that, in comparison to wild-type (WT) animals, *Fhl2*-targeted knockout (KO) mice showed exaggerated cardiac hypertrophy in response to chronic isoprenaline infusion [11,13].

In order to identify novel interaction partners for FHL2 in the heart, which could expand the understanding of the biological roles of this protein, a yeast 2-hybrid screen was performed prior to this study using a human cardiac cDNA library and human *FHL2* as a bait [14]. This screen identified cardiomyopathy-associated 5 (CMYA5, also called myospryn) as a potential novel FHL2 interaction partner. Like FHL2, CMYA5 is described to function as a scaffold protein [15,16]. CMYA5 is mainly expressed in muscle tissues [17], and in humans, the *CMYA5* gene encodes a protein of 4069 amino acids (aa; UniProt identifier number: Q8N3K9). The defined structural domains of CMYA5 are localised in its C-terminus involving a truncated tripartite motif (TRIM), which includes a B-box' (a variant of B-Box-type zinc finger), a B-box coiled coil (BBC), two fibronectin type-III (FNIII) and a SPI α and ryanodine receptor (SPRY) domain [15,16,18] (Fig. 1A). *CMYA5* expression is reduced in skeletal muscles from patients with Duchenne muscular dystro-

Fig. 1. FHL2 interacts with the N- and C-terminal regions of CMYA5. (A) Illustration of the human CMYA5 protein. BBC: B-box coiled-coil; FN: fibronectin type-III domain; SPRY: SPIA and RYanodine receptor domain. (B) 500-aa-long moieties of human CMYA5 (C-terminal: 569 aa) were expressed as recombinant V5/His₆-tagged proteins. The purified recombinant V5/His₆-tagged CMYA5 proteins were resolved by SDS/PAGE and detected by immunoblotting using an anti-V5 antibody and Coomassie staining. The recombinant protein corresponding to aa2501–3000 was not expressed. (C) Purified recombinant GST and GST-FHL2 were resolved by SDS/PAGE and detected by immunoblotting using an anti-GST antibody. Following this, the membrane was stained with Coomassie stain. (D) The recombinant V5/His₆-tagged CMYA5 proteins were used in *in vitro* GST pull-down assays to investigate which CMYA5 region interacts (+) or not (–) with recombinant GST-tagged human FHL2. For the assays, V5/His₆-tagged CMYA5 proteins (400 pmol) were incubated for 1 h with GST-FHL2 (200 pmol) or, as control, with GST (200 pmol) or glutathione-sepharose beads only (b.). Immunoblot analysis using an anti-V5 antibody was used to assess interaction between the recombinant V5/His₆-CMYA5 proteins and GST-FHL2. Content of the GST-tagged proteins in each pull-down reaction was detected with an anti-GST antibody. The immunoblot analysis demonstrated interaction of GST-FHL2 with recombinant proteins corresponding to the CMYA5 N-terminus (aa1–500) and C-terminus (aa3501–4069). Immunoblots are representative of at least three independent experiments. ?: unknown, whether this CMYA5 region interacts with GST-FHL2 since recombinant protein could not be expressed.



phy and the corresponding humanised mdx mouse model [17,19]. Additionally, *CMYA5* polymorphisms have been associated with the onset of hypertrophic cardiomyopathy (HCM) [20,21] and incidences of schizophrenia [21,22]. With this study, we aimed to characterise the interaction between FHL2 and CMYA5 in a cardiac myocyte context.

Results

FHL2 interacts with the N- and C-terminal regions of CMYA5

To determine whether FHL2 and CMYA5 are binding partners, their interaction was investigated *in vitro*. For this purpose, eight nonoverlapping V5/His₆-tagged moieties of human CMYA5 were cloned to cover the entire CMYA5 protein sequence: seven moieties comprised 500-aa-long protein regions and one the C-terminal 569 aa of CMYA5. Of these recombinant proteins, it was not possible to purify the CMYA5 fragment encompassing CMYA5 aa2501–3000 (Fig. 1B). The expected molecular mass of these proteins ranged between 50 and 60 kDa. However, analysis by SDS/PAGE revealed deviating migration patterns compared to their expected molecular mass, which might be attributed to protein conformation, incomplete denaturation in sample buffer or post-translational modifications (Fig. 1B). Subsequently, *in vitro* interaction of FHL2 with individual recombinant CMYA5 proteins was investigated by glutathione-S-transferase (GST) pull-down assays using recombinant GST-FHL2 or, as control, GST alone. Expression of purified GST and GST-FHL2 proteins is shown in Fig. 1C. As an additional control in this experiment, recombinant V5/His₆-CMYA5 proteins were incubated with glutathione-sepharose beads alone. Immunoblot analysis of the pull-down fractions using an anti-V5 antibody showed background binding of the recombinant CMYA5 proteins to the beads or to GST alone, apart from V5/His₆-CMYA5_(3501–4069). However, GST-FHL2 was efficiently coprecipitated with recombinant proteins corresponding to aa1–500 and aa3501–4069 of CMYA5 (Fig. 1D) when

compared to the GST control or the beads-only samples. Hence, FHL2 interacted with CMYA5 and this occurred via the CMYA5 N- and C-terminal regions.

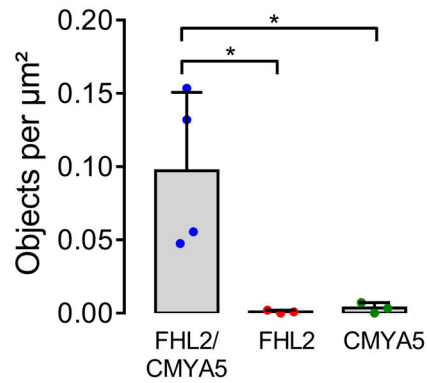
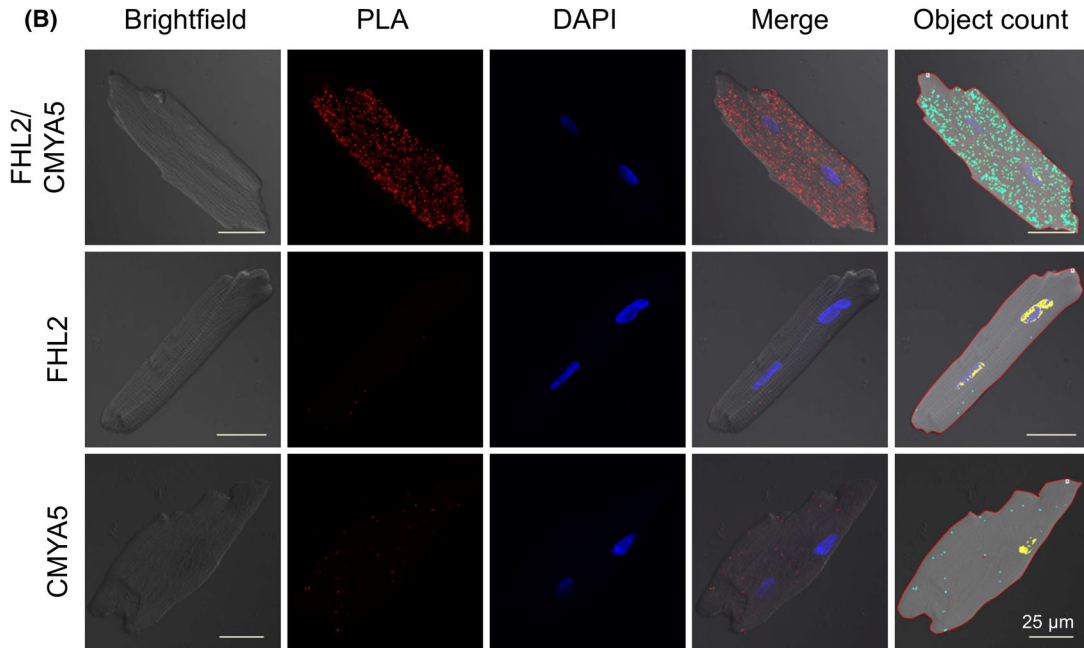
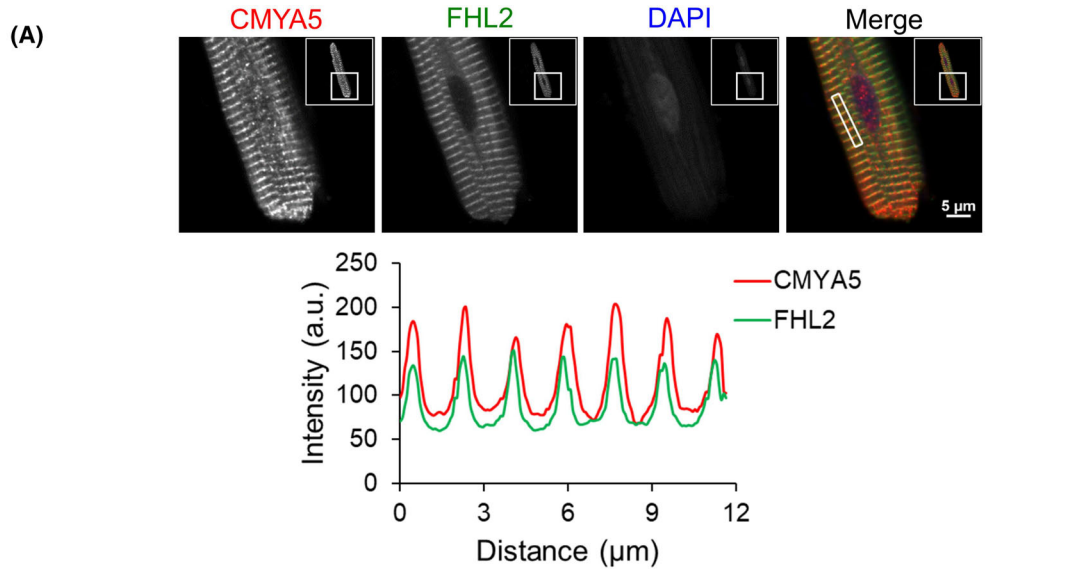
FHL2 and CMYA5 colocalise in cardiac myocytes

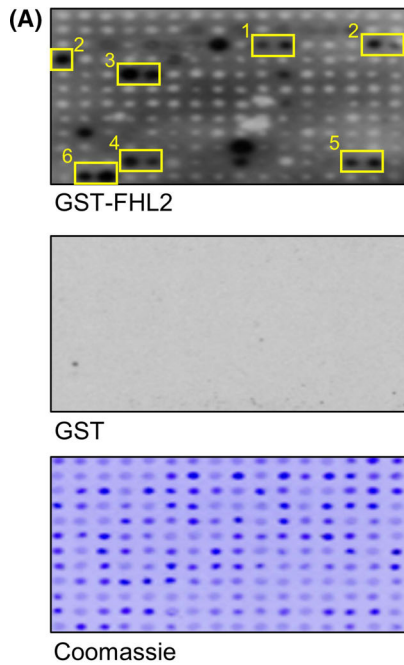
To analyse FHL2 and CMYA5 in a cardiac myocyte context, immunofluorescence experiments were performed in adult rat ventricular myocytes (ARVM). This revealed a specific striated pattern for both proteins in the subregion of the Z-disc as shown also by plotting the fluorescence intensity profile for the two proteins (Fig. 2A). This occurs in agreement with previous work that had demonstrated an association of CMYA5 with α -actinin as well as the ryanodine receptor 2 (RyR2) at the cardiac dyad in the Z-disc region [23,24]. To demonstrate the close association between FHL2 and CMYA5 in cardiac myocytes, *in situ* proximity ligation assay (PLA) by Duolink™ was performed. Incubation of ARVM with either anti-FHL2 or anti-CMYA5 antibody alone did not result in positive PLA signals (Fig. 2B). In contrast, concurrent incubation of cardiac myocytes with both antibodies produced significantly increased signal intensities for PLA (Fig. 2B), supporting the *in vitro* observation of a direct interaction between FHL2 and CMYA5 *in cellulo*.

Identification of CMYA5 peptide sequences that interact with FHL2

To investigate the interaction interface between CMYA5 and FHL2, a peptide array built of 25-aa-long overlapping peptides shifted by 5 aa, corresponding to the CMYA5 N- and C-termini, was performed. The peptides were synthesised on a cellulose membrane using the SPOT synthesis method described in the “Materials and methods” section and incubated with either recombinant GST-FHL2 or GST protein alone, and the interaction was investigated with an anti-GST antibody (Fig. 3A). Positive interactions worthy of further investigation were considered as those that spanned at least two consecutive 25mer spots on the membrane after incubation with recombinant GST-FHL2 and no signal after incubation with recombinant

Fig. 2. Interaction of FHL2 and CMYA5 in ARVM. (A) ARVM were fixed in 4% (v/v) PFA and immunostained with antibodies recognising FHL2 (green) and CMYA5 (red). Following staining with fluorescent secondary antibodies (anti-mouse Alexa Fluor™ 488 and anti-rabbit Dylight™ 549), cells were imaged under a confocal microscope. DAPI was used to stain the nuclei. The diagram depicts the fluorescence intensity profile corresponding to FHL2 and CMYA5 staining in the rectangular area shown in the right merged image. (B) ARVM were subjected to a PLA using the Duolink™ methodology. Cells were incubated with a combination of anti-FHL2 and anti-CMYA5 antibodies or with each antibody alone as control. Positive PLA signals appear red. Object count was performed digitally after a signal intensity threshold was defined automatically. Each counted signal is displayed as turquoise spot in the ‘Object count’ image. Data were expressed as Object counts· μm^{-2} . Number of cells: FHL2 + CMYA5 = 4; FHL2 alone/CMYA5 alone = 3. * $P < 0.05$. Scale bar = 25 μm .





#	aa	Sequence
1	206–235	GAIYKEHKPLVLRPVYIGTVQYKIKMFNSV
2	231–265	MFNSVKEELIPLQFYGTLPKGYVIKEIHYRKGKDA
3	336–365	SALEHTVPSYSSSGRAEQGIQLRHSQSV PQ
4	3836–3865	YTLEYCRQHSPEGEGLRSFSGIKGLQLKVN
5	3886–3915	EQSEAALISTRGTRFLLLRETAHPALHISS
6	3906–3935	TAHPALHISSSGTVISFGERRRLTEIPSVL

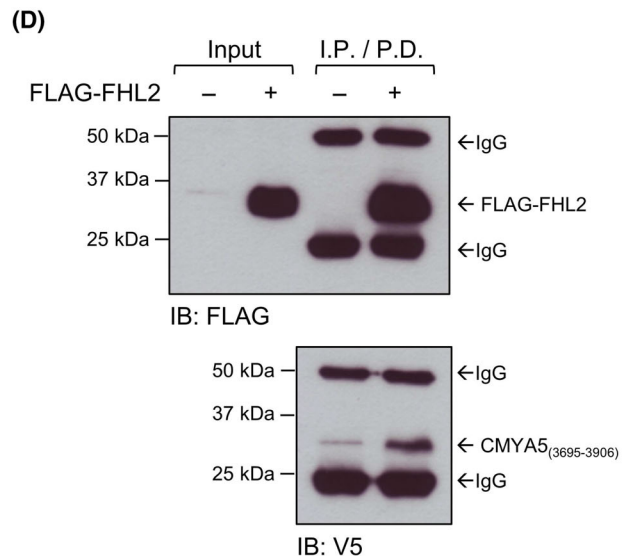
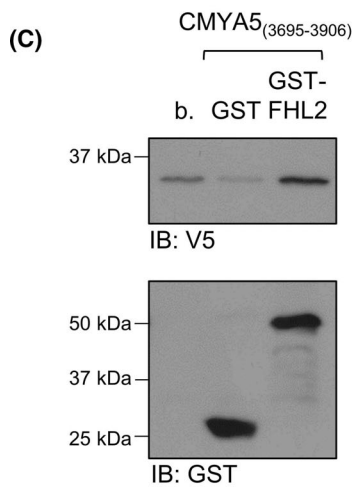
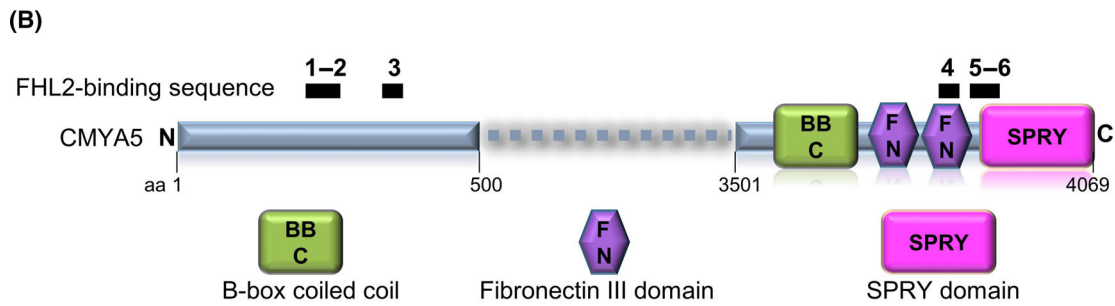


Fig. 3. Identification of CMYA5 peptide sequences interacting with FHL2. (A) A peptide array assay was used to identify the CMYA5 peptide interface that interacts with FHL2. The CMYA5 N- and C- termini were expressed as overlapping 25-aa peptides spotted on cellulose membrane. The membrane was incubated with recombinant GST-FHL2 or GST as control, followed by incubation with anti-GST and anti-mouse secondary antibodies. Peptide spotting was assessed with Coomassie stain of the membrane. CMYA5 sequences interacting with FHL2 are shown in the table. (B) Illustration of the topology of the FHL2-interacting sequences on CMYA5 protein. BBC: B-box coiled-coil; FN: fibronectin type-III domain; SPRY: SPIA and RYanodine receptor domain. (C) Recombinant GST-FHL2 (200 pmol) was incubated with a recombinant V5/His₆-tagged human CMYA5 protein encompassing the two FNIII domains of CMYA5 (V5/His₆-CMYA5_(3695–3906); 400 pmol). As control, V5/His₆-CMYA5_(3695–3906) was incubated with either recombinant GST (200 pmol) or glutathione-sepharose beads only (b.). Interaction between V5/His₆-CMYA5_(3695–3906) and GST-FHL2 was assessed by immunoblot analysis using an anti-V5 antibody. Immunoblotting with an anti-GST antibody demonstrated the content of the GST-tagged proteins in the pull-down reactions. (D) FLAG-tagged FHL2 was expressed in HEK293T cells, immunoprecipitated using anti-FLAG resin and then incubated with 100 pmol V5/His₆-CMYA5_(3695–3906). Pull-down of recombinant V5/His₆-CMYA5_(3695–3906) by immunoprecipitated FLAG-FHL2 (fraction I.P./P.D.) was investigated by immunoblotting with an anti-V5 antibody. Lysates from cells that did not express FLAG-FHL2 were used as control. FLAG-FHL2 in lysate inputs and the I.P./P.D. fractions was detected with an anti-FLAG antibody. Immunoblots in C-D are representative of at least three independent experiments. IgG: anti-FLAG immunoglobulin-G chain.

GST. Six such positive areas of interaction were observed representing aa206–265 and aa336–365 in the CMYA5 N-terminus and aa3836–3865 and aa3886–3935 in the CMYA5 C-terminus as the putative binding interface with FHL2 (Fig. 3A,B). The C-terminal sequences belonged to the second FNIII and the SPRY domains of CMYA5 and, therefore, might be responsible for the association of FHL2 with that region of CMYA5 (Fig. 3B).

The preference of FHL2 to interact with FNIII domains has been previously shown for the binding of FHL2 to cardiac myosin-binding protein C [25]. To further confirm the interaction of FHL2 with the FNIII domains of CMYA5, the GST pull-down assay was repeated using a recombinant V5/His₆-tagged protein that encompasses only the two FNIII CMYA5 domains (V5/His₆-CMYA5_(3695–3906)). Immunoblot analysis with an anti-V5 antibody showed robust detection of V5/His₆-CMYA5_(3695–3906) in the GST-FHL2 pull-down sample compared to the control samples, which confirmed an interaction between the CMYA5 FNIII domains and FHL2 (Fig. 3C). This *in vitro* observation was corroborated in a mammalian expression system. FLAG-FHL2 was expressed in HEK293T cells, immunoprecipitated with an anti-FLAG resin and then incubated with recombinant V5/His₆-CMYA5_(3695–3906). Lysates from nontransfected cells served as control. Immunoblot analysis with an anti-V5 antibody revealed enrichment of V5/His₆-CMYA5_(3695–3906) in the sample containing immunoprecipitated FLAG-FHL2 compared to the control lysate (Fig. 3D). Together, these data demonstrated the propensity of FHL2 to associate with FNIII structural domains and confirmed the observation from the peptide spot array that FHL2 interacted with the FNIII domains of CMYA5.

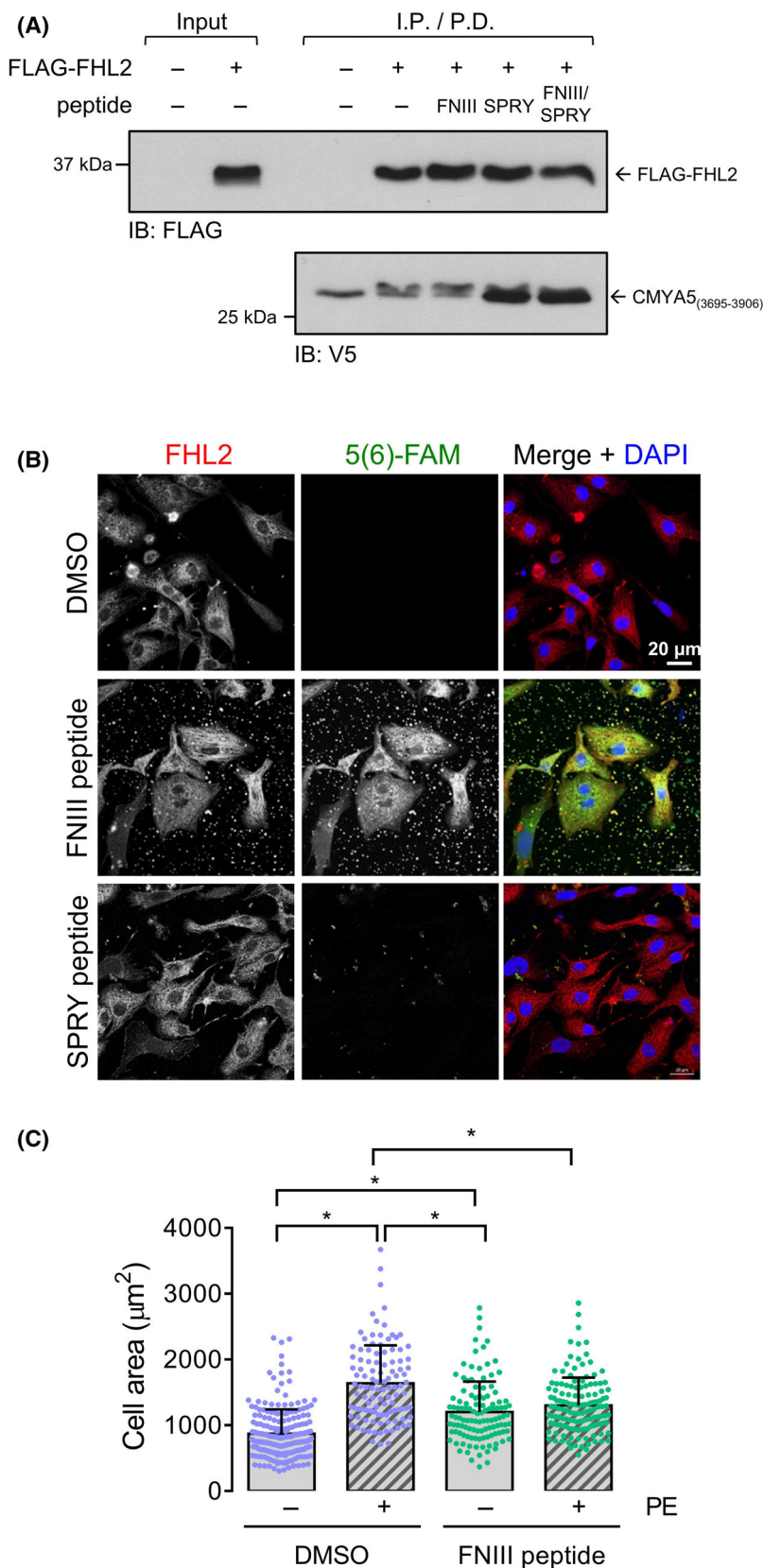
Application of the FNIII peptide affects cardiac myocyte size

Peptide sequences corresponding to binding motifs in peptide arrays can be employed as a tool to modulate the protein–protein interaction and to investigate its biological significance [26]. Therefore, 25-aa-long peptides encompassing parts of the second FNIII domain [part of peptide #4 (FNIII peptide); sequence: YTLEYCRQHSPEGEGLRSFSGIKGL] and the SPRY domain (part of peptide #6 (SPRY peptide); sequence: LQISSNGTVISFERRRLTEIPSVL; adjusted to the corresponding rat sequence) of CMYA5 were synthesised. Due to limited resources, peptides corresponding to the FHL2-binding interface of the CMYA5 N-terminus were not tested in this study. Initially, peptides were used in *in vitro* competition assays and subsequently administered to cardiac myocyte cultures. Therefore, peptides were N-myristoylated to enhance sarcolemma permeation and conjugated to 5(6)-carboxyfluorescein (5(6)-FAM) to monitor access into the cardiac myocytes by confocal microscopy [27].

To test whether the peptides could interfere with the interaction between FHL2 and CMYA5 *in vitro*, immunoprecipitated FLAG-FHL2 was incubated with V5/His₆-CMYA5_(3695–3906) in the presence of either the FNIII or SPRY peptide or a combination of both (Fig. 4A). Western immunoblot analysis revealed no competition of the FLAG–FHL2 interaction with V5/His₆-CMYA5_(3695–3906) by addition of the peptides (Fig. 4A). This could be due to the experimental assay conditions.

Nevertheless, the effect of peptide exposure on cultured cardiac myocytes was investigated. Neonatal rat ventricular myocytes (NRVM) were incubated for 8 h with either peptide (10 μmol·L⁻¹) and 5(6)-FAM fluorescence was assayed. Image analysis demonstrated that the FNIII

Fig. 4. Effect of the FNIII peptide on cardiac myocyte hypertrophy. (A) FLAG-tagged FHL2 was expressed in HEK293T cells, immunoprecipitated using anti-FLAG resin and then incubated with 10 pmol V5/His₆-CMYA5₍₃₆₉₅₋₃₉₀₆₎ in the presence of either the FNIII peptide (10 nmol; relates to peptide #4 in Fig. 3), the SPRY peptide (10 nmol; relates to peptide #6 in Fig. 4), a combination of the FNIII (5 nmol) and SPRY (5 nmol) peptides or DMSO as control. The binding of recombinant V5/His₆-CMYA5₍₃₆₉₅₋₃₉₀₆₎ to immunoprecipitated FLAG-FHL2 (fraction I.P./P.D.) was investigated by immunoblotting with an anti-V5 antibody. Lysates from cells that did not express FLAG-FHL2 and incubated with V5/His₆-CMYA5₍₃₆₉₅₋₃₉₀₆₎ and DMSO were used as additional control. FLAG-FHL2 in lysate inputs and the I.P./P.D. fractions was detected with an anti-FLAG antibody. Immunoblots are representative of three independent experiments. (B) NRVM were exposed for 8 h to DMSO or FHL2-binding peptides corresponding to the second FNIII (FNIII peptide; 10 $\mu\text{mol}\cdot\text{L}^{-1}$) and the SPRY (SPRY peptide; 10 $\mu\text{mol}\cdot\text{L}^{-1}$) domains of CMYA5. The peptides were N-terminally myristoylated and labelled at the C-terminus with 5(6)-FAM to allow cellular uptake and visualisation respectively. Cells were then fixed in 4% (v/v) PFA and immunostained with an anti-FHL2 antibody followed by incubation with anti-rabbit DyLight™ 549 secondary antibody. Nuclei were stained with DAPI. Observation was performed under a confocal microscope. Evaluation of the peptide's cell permeance was performed using the excitation/emission settings as for Alexa Fluor™ 488. (C) NRVM were pre-incubated for 7 h with DMSO (5 μL) or 5 $\mu\text{mol}\cdot\text{L}^{-1}$ myristoylated FNIII peptide and then exposed to 10 $\mu\text{mol}\cdot\text{L}^{-1}$ PE. Control cells did not receive PE. 24 h later a quarter of medium was removed and DMSO, peptide and PE were re-applied for another 24 h. The cumulative final concentration of the peptide was 8.75 $\mu\text{mol}\cdot\text{L}^{-1}$. NRVM cell area (in μm^2) was evaluated by confocal microscopy after staining with DyLight™ 633-labelled phalloidin, α -actinin and DAPI and images were analysed with ImageJ. Cell numbers per condition: DMSO = 211; DMSO + PE = 109; FNIII peptide = 117; FNIII peptide + PE = 136. * $P < 0.05$.



peptide could efficiently enter the NRVM, whereas fluorescence of the SPRY peptide was not detectable (Fig. 4B). Subsequent experiments focused therefore on investigating the phenylephrine (PE)-induced prohypertrophic response in NRVM after pre-incubation with the FNIII peptide. For this, NRVM were exposed to DMSO or FNIII peptide ($8.75 \mu\text{mol}\cdot\text{L}^{-1}$ final cumulative concentration), and treated with or without PE for 48 h. As expected, in DMSO-treated NRVM, exposure to PE caused an increase in cardiac myocyte cell area compared to cells cultured under control conditions (DMSO/–PE: $870.4 \pm 371 \mu\text{m}^2$ vs DMSO/+PE: $1639.0 \pm 576.6 \mu\text{m}^2$). NRVM exposed to the FNIII peptide under basal conditions displayed a significantly increased cell area compared to DMSO-treated cells (DMSO/–PE: $870.4 \pm 371.0 \mu\text{m}^2$ vs FNIII/–PE: $1201.0 \pm 464.6 \mu\text{m}^2$; Fig. 4C). Importantly, in NRVM stimulated with PE, prior exposure to the FNIII peptide significantly reduced the PE-induced prohypertrophic response observed in DMSO-treated NRVM (DMSO/

+PE $1639.0 \pm 576.6 \mu\text{m}^2$ vs FNIII/+PE: $1300.0 \pm 423.9 \mu\text{m}^2$; Fig. 4C). Thus, incubation with the FNIII peptide protects from PE-induced hypertrophy.

Association of FHL2 expression with *Cmya5* transcript levels

Prohypertrophic stimuli, like PE, increase *Cmya5* gene expression in cardiac myocytes [28] and an important biological role of FHL2 is to coregulate transcription factor activity [29]. To investigate whether FHL2 impacts on *Cmya5* gene expression, *Cmya5* transcription levels were assessed in NRVM expressing either native FHL2 (\emptyset virus) or FLAG-tagged FHL2 after adenoviral-mediated gene transfer (Ad5:FLAG-*Fhl2*). Additionally, NRVM were treated with vehicle (PBS) or PE as a prohypertrophic stimulus for 48 h. FLAG-*Fhl2* overexpression was verified by immunoblot analysis using anti-FHL2 and anti-FLAG antibodies (Fig. 5A). Compared to nontransduced NRVM,

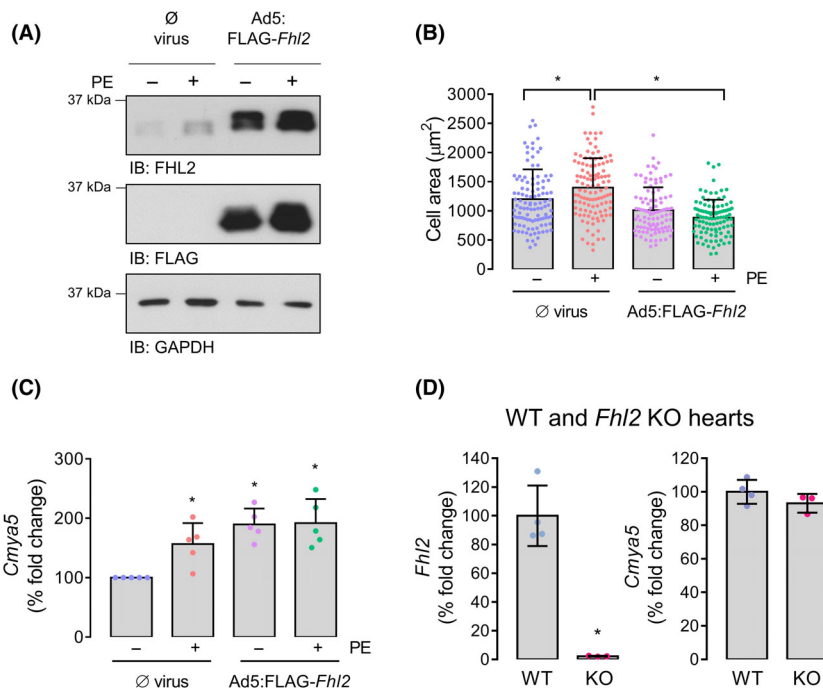


Fig. 5. Effect of changes in FHL2 levels on *Cmya5* mRNA levels. (A) NRVM overexpressing FLAG-tagged FHL2 by means of adenoviral gene transfer (Ad5:FLAG-*Fhl2*) were left untreated or exposed to PE ($10 \mu\text{mol}\cdot\text{L}^{-1}$) for 48 h. Untransduced NRVM (\emptyset virus) subjected to identical treatments were used as control. Verification of heterologous FHL2 overexpression was done by immunoblot analysis using anti-FHL2 and anti-FLAG antibodies. Immunodetection of GAPDH was used as loading control. (B) Measurement of cardiac myocyte cell area (in μm^2) in response to PE and FHL2 overexpression was performed by analysing confocal microscope images with Image J. $*P < 0.05$. Number of cells measured: \emptyset virus/–PE = 110; \emptyset virus/+PE = 113; Ad5: FLAG-*Fhl2*/–PE = 99; Ad5:FLAG-*Fhl2*/+PE = 103. (C) Investigation of *Cmya5* expression in response to PE and FHL2 overexpression. Data ($N = 5$) were normalised to *Gnas* mRNA levels and are expressed as % fold change over the untransduced control (\emptyset virus/–PE). $*P < 0.05$ compared to untransduced control. (D) *Fhl2* and *Cmya5* expression was investigated in hearts from WT ($N = 4$) or *Fhl2*-targeted KO mice ($N = 3$). mRNA expression levels were normalised to *Gnas* transcript levels. Scatter plots demonstrate data as % fold change over the average expression in WT hearts. $*P < 0.05$ vs WT.

transduction with Ad5:FLAG-*Fhl2* resulted in an approximately 10-fold higher FHL2 protein level (Fig. 5A). Exposure of NRVM to PE significantly increased cell area (\emptyset virus/–PE: $1201 \pm 48 \mu\text{m}^2$ vs \emptyset virus/+PE: $1400 \pm 47 \mu\text{m}^2$) as expected and this response was blunted by FHL2 overexpression (Ad5:FLAG-*Fhl2*/+PE: $884 \pm 30 \mu\text{m}^2$; Fig. 5B).

To investigate the impact of FHL2 overexpression on *Cmya5* gene expression, *Cmya5* mRNA levels were analysed by RT-quantitative PCR (qPCR). Compared to control-treated NRVM, PE induced a significant increase in *Cmya5* mRNA levels in nontransduced NRVM (\emptyset virus/+PE: $156.7\% \pm 35.2\%$ over the \emptyset virus/–PE; Fig. 5C). Interestingly, overexpression of FHL2 was sufficient to enhance *Cmya5* gene expression (Ad5:FLAG-*Fhl2*/–PE: $189.6\% \pm 26.7\%$ over the \emptyset virus/–PE) and further treatment of the Ad5:FLAG-*Fhl2*-transduced NRVM with PE did not further increase *Cmya5* transcription levels (Ad5:FLAG-*Fhl2*/+PE: $191.9\% \pm 40.3\%$ over the \emptyset virus/–PE; Fig. 5C). This result suggested that FHL2 might impact on *Cmya5* gene expression.

Knockout of FHL2 impacts on CMYA5 localisation

To further investigate this observation, gene expression of *Cmya5* was analysed in hearts from WT and *Fhl2*-targeted KO mice and this showed similar *Cmya5* mRNA levels in both genotypes (Fig. 5D).

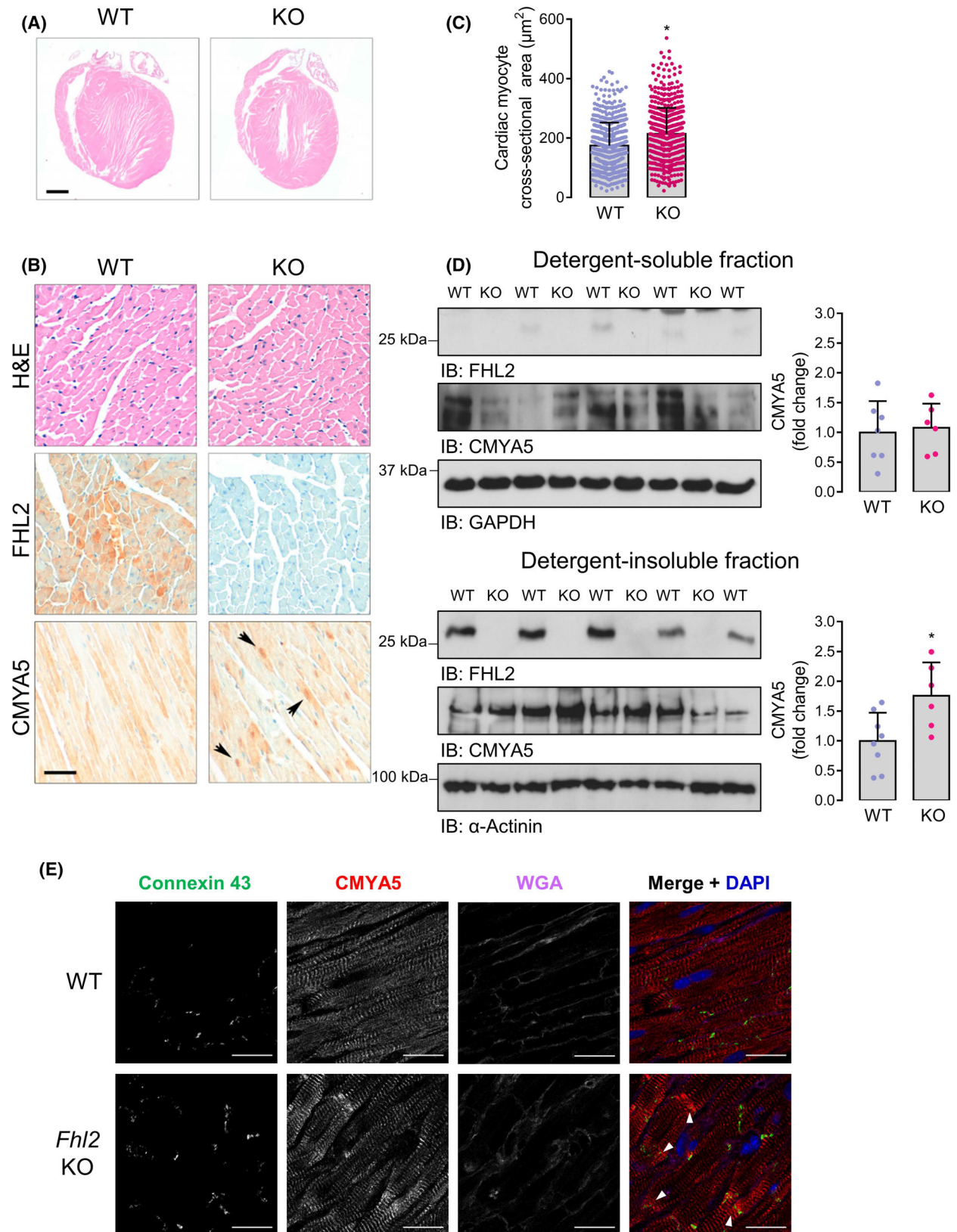
Next, histological analysis of heart sections from WT and *Fhl2* KO mice was performed. Staining with haematoxylin and eosin (H&E) did not reveal obvious morphological differences between the two genotypes (Fig. 6A,B). Dystrophin staining unveiled significantly higher cross-sectional area of *Fhl2* KO than WT cardiac myocytes (*Fhl2* KO: $214.5 \pm 3.5 \mu\text{m}^2$ vs WT: $174.8 \pm 3.2 \mu\text{m}^2$; Fig. 6C). The absence of FHL2 in *Fhl2* KO mouse sections was confirmed by staining with an anti-FHL2 antibody (Fig. 6B). CMYA5

staining by immunohistochemistry revealed distinct accumulation of CMYA5 in the perinuclear area only in heart sections from *Fhl2* KO mice (Fig. 6B, arrowheads). This observation was paralleled by higher CMYA5 protein levels in the detergent-insoluble fraction of *Fhl2* KO heart homogenates compared to the respective WT samples (Fig. 6D). This fraction contains detergent-insoluble cellular components such as myofilament and myofilament-associated proteins [30]. Cryosections from WT and *Fhl2* KO hearts were also analysed by immunofluorescence and confocal microscopy. Staining of these heart sections with an anti-CMYA5 antibody showed a striated pattern for CMYA5 in both, WT and *Fhl2* KO heart sections (Fig. 6E). In *Fhl2* KO heart sections, the striated CMYA5-corresponding pattern was weaker compared to WT sections and instead higher fluorescence intensity was detectable at the intercalated disc region and gap junctions, indicated by costaining with an anti-connexin 43 antibody (Fig. 6E, arrowheads). Therefore, these data suggest an impact of FHL2 on the subcellular distribution of CMYA5.

CMYA5 in the *Mybpc3* knock-in mouse model of HCM

We additionally investigated expression and localisation of CMYA5 in a humanised knock-in (KI) mouse model of HCM carrying a patient mutation in *MYBPC3*, that exhibits reduced FHL2 mRNA and protein levels [4]. In agreement with these data, *Fhl2* transcript levels were 60% lower in the KI than in WT hearts (Fig. 7A). Notably, this was accompanied by an approximately 20% reduction in the *Cmya5* mRNA levels in the *Mybpc3* KI heart samples (Fig. 7A). Additionally, immunofluorescence analysis of FHL2 and CMYA5 localisation was performed in cryosections from WT and *Mybpc3* KI hearts. In WT hearts, immunofluorescence signals for both FHL2 and

Fig. 6. *Cmya5* expression and localisation in *Fhl2*-targeted KO mouse hearts. (A) Representative H&E staining of WT and *Fhl2*-targeted KO hearts show no gross abnormalities in *Fhl2* KO; scale bar: 1000 μm . (B) Histological and immunohistochemical analyses of WT and *Fhl2* KO heart tissue are shown. Representative images display the loss of FHL2 in hearts of *Fhl2* KO mice. While total expression level of CMYA5 in heart tissue is not changed by the KO of *Fhl2*, we detected specific accumulation of CMYA5 to the perinuclear region in the KO hearts (see black arrows); scale bar: 50 μm . (C) Cardiac myocyte cross-sectional area was measured in dystrophin-stained heart sections from WT ($N = 568$ myocytes) or *Fhl2* KO ($N = 608$ myocytes) mice. (D) CMYA5 protein levels in the detergent-soluble and -insoluble fractions of homogenates from WT ($N = 7$) or *Fhl2*-targeted KO ($N = 6$) mouse hearts were analysed by immunoblotting using an anti-CMYA5 antibody. Immunodetection of GAPDH and α -actinin were used as loading controls for the soluble and insoluble fraction respectively. Scatter plots represent data normalised to the respective loading control and expressed as fold-change over the average WT level. * $P < 0.05$ vs WT. (E) Detection of CMYA5 in *Fhl2*-targeted KO mouse hearts by immunofluorescence and confocal microscopy. Cryosections of hearts from WT or *Fhl2* KO were stained with anti-CMYA5 (red) and anti-connexin 43 (green) antibodies. Nuclei and plasma membranes were stained with DAPI (blue) and WGA (purple) respectively. Arrowheads indicate accumulation of CMYA5 at intercalated disc region. Scale bars: 20 μm .



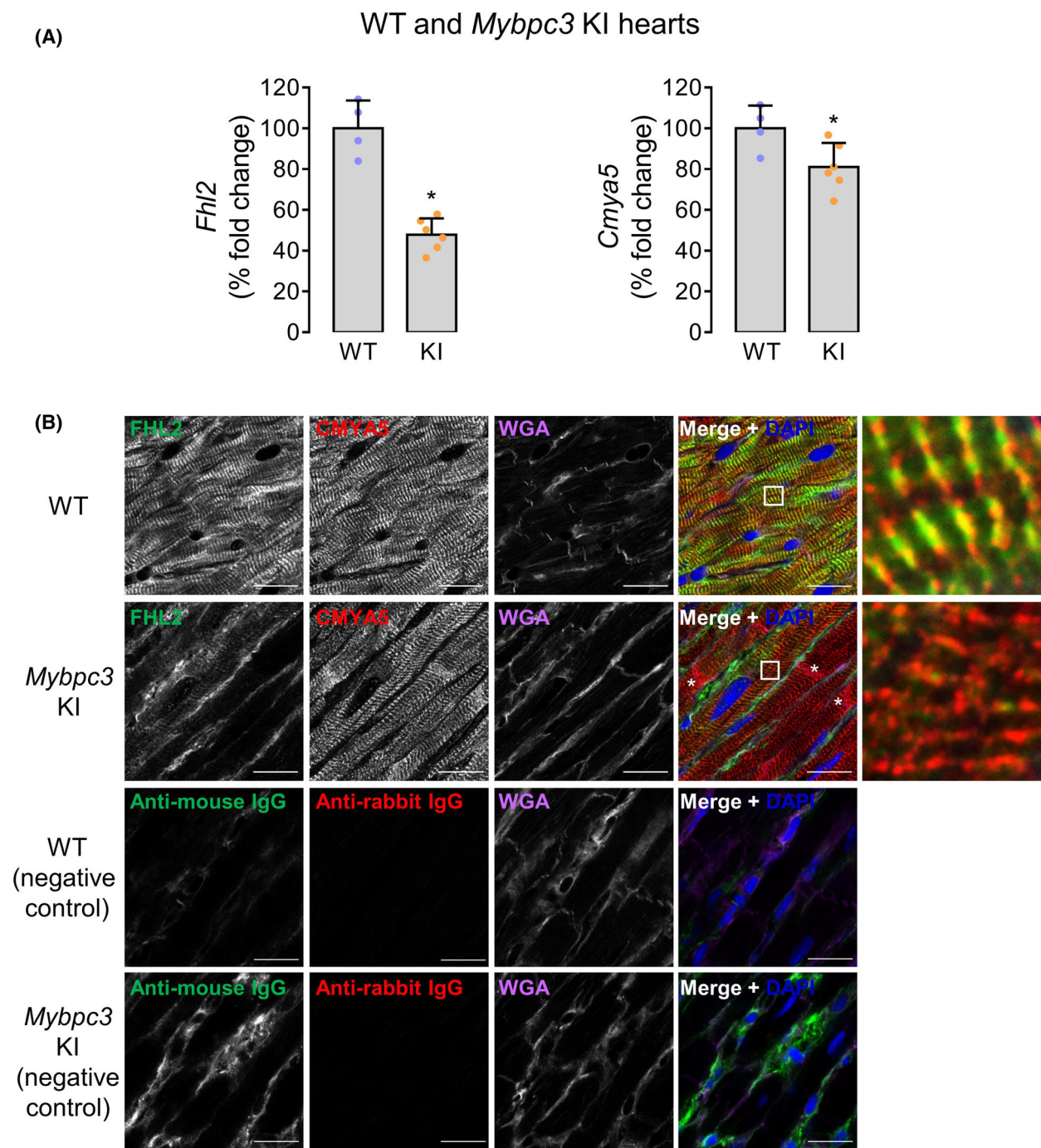


Fig. 7. *Fhl2* and *Cmya5* expression in hearts from WT and *Mybpc3* KI mice. (A) *Fhl2* and *Cmya5* expression was investigated in hearts from WT ($N = 4$) or *Mybpc3* c.772G>A KI mice ($N = 6$). mRNA expression levels were normalised to *Gnas* transcript levels. Scatter plots demonstrate data as % fold change over the average expression in WT hearts. $P < 0.05$ vs WT. (B) Cryosections of hearts from WT or *Mybpc3* KI mice were immunostained with anti-FHL2 (green) and anti-CMYA5 (red) antibodies. Nuclei and plasma membranes were stained with DAPI (blue) and WGA (purple) respectively. Control sections were stained with secondary antibodies only. Please note the increased nonspecific binding of the anti-mouse secondary antibody in the *Mybpc3* KI heart sections. The images in the last column are magnifications of the selected areas (squares) shown in the merged-channels images. Asterisks (*) indicate accumulation of CMYA5 at intercalated discs. Scale bars: 20 μ m.

CMYA5 revealed a striated co-localised pattern (Fig. 7B), as observed previously in isolated ARVM (Fig. 2A). No complete overlay of the FHL2 and CMYA5 immunofluorescence signals was detectable indicating that only a proportion of the FHL2 and CMYA5 protein localises in vicinity. In *Mybpc3* KI heart sections, CMYA5 maintained its striated pattern, whilst the immunofluorescence signal corresponding to FHL2 was strongly attenuated (Fig. 7B) reflecting the reduction in *Fhl2* gene expression and protein levels shown before in these animals [4]. Furthermore, the reduction in FHL2 levels in *Mybpc3* KI heart sections was accompanied by a redistribution and intercalated disc accumulation for CMYA5 (Fig. 7B, asterisks),

suggesting that FHL2 might be needed for subcellular targeting of CMYA5 to the Z-disc regions in cardiac myocytes.

Finally, because CMYA5 associates with RyR2 at the cardiac dyads [23], a possible colocalisation of FHL2 with RyR2 or junctophilin 2 (JPH2), another protein component of the dyad complex [31], was investigated by confocal microscopy in WT and *Mybpc3* KI heart sections (Fig. 8). In WT hearts, the immunofluorescence for RyR2 and JPH2 had a punctate striated pattern, whereas this was disorganised in the *Mybpc3* KI heart sections. Analysis of FHL2 immunofluorescence showed no overlap with the signals for RyR2 (Fig. 8A) or JPH2 (Fig. 8B) in both

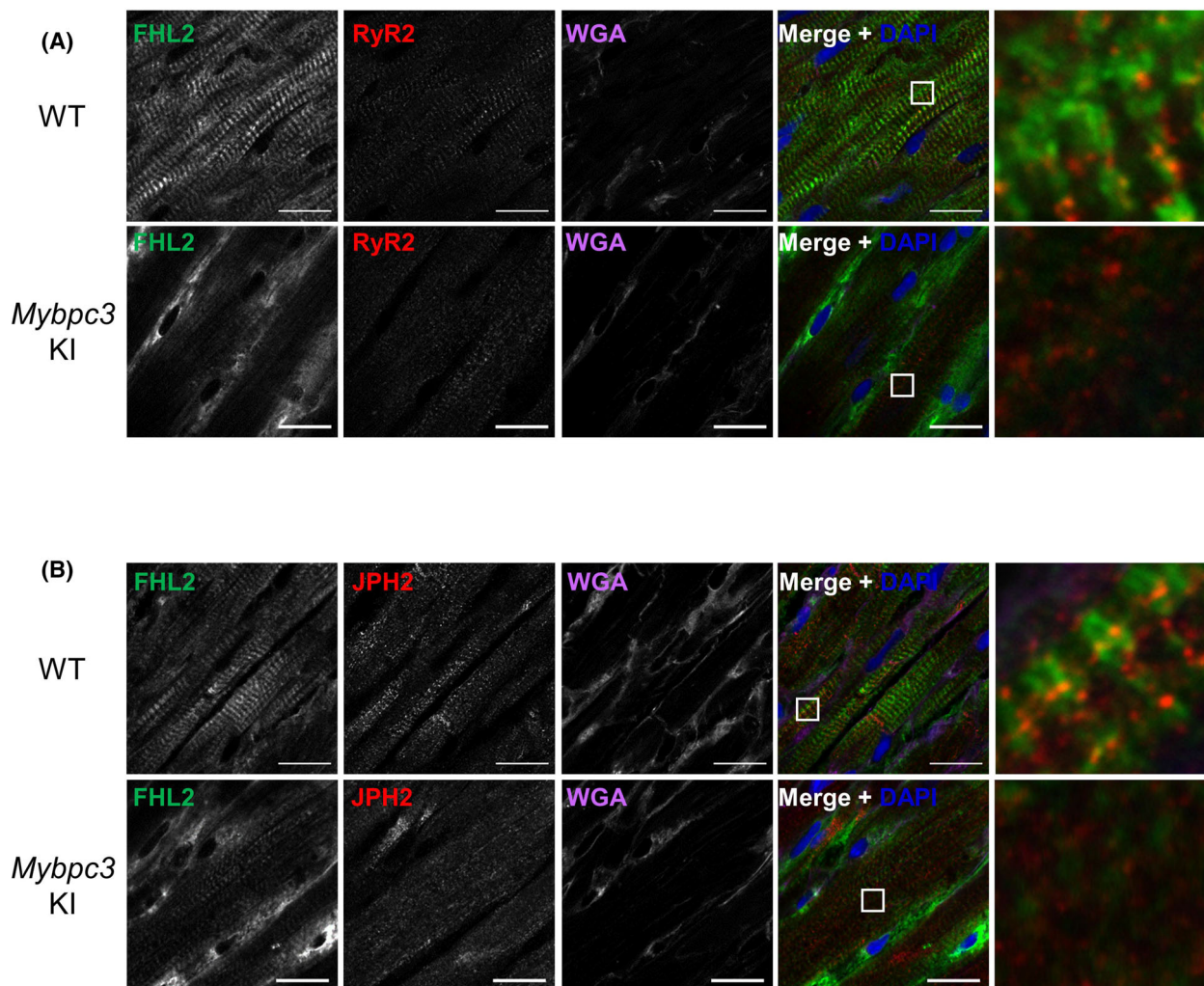


Fig. 8. FHL2 does not localise to the cardiac dyad. Cryosections of hearts from WT or *Mybpc3* KI mice were immunostained with anti-FHL2 (green) and anti-RyR2 (red) (A) or anti-JPH2 (red) (B) antibodies. Nuclei and plasma membranes were stained with DAPI (blue) and WGA (purple) respectively. The images in the last column are magnifications of the selected squared areas shown in the merged-channels images. Scale bars: 20 μm.

WT and *Myhpc3* KI heart sections, indicating lack of association of FHL2 with the cardiac dyad complex.

Taken together, the above data suggest a functional relationship between the two adaptor proteins FHL2 and CMYA5 in cardiac myocytes, in which FHL2 impacts on subcellular compartmentation and possibly expression of CMYA5.

Discussion

FHL2 is an adaptor protein with high expression in heart tissue [32], and reduced abundance in human heart failure and in animal models of heart disease [3–7]. The biological roles of FHL2 are defined by its protein interaction partners. It is known that FHL2 regulates integrin signalling [33,34], enzyme activity and subcellular location [8–12]. Furthermore, it functions as a transcriptional co-activator or repressor, a role dependent on the associated transcription factor [29,35–37].

In the present study, we demonstrated that FHL2 interacts with CMYA5, a cytoskeletal protein reported to localise at the cardiac myocyte costameres, sarcomeres, intercalated discs, the perinuclear region and in association with the sarcoplasmic reticulum [23,38–40]. The exact subcellular localisation of CMYA5 in cardiac myocytes is, however, a matter of debate. For example, Durham *et al.* [24] reported interaction of CMYA5 with the Z-line protein α -actinin, which was contested by the study of Benson *et al.* [23] that showed lack of co-immunoprecipitation (IP) of the two proteins. On the other hand, the latter study concluded that CMYA5 is part of the cardiac dyads by directly interacting with RyR2 [23]. This finding was corroborated by the identification of CMYA5 as a proximal protein to JPH2 [41], which together with RyR2 are components of the cardiac dyads [31]. Our confocal microscopy analysis performed in ARVM and mouse hearts revealed a punctate striated immunostaining pattern for CMYA5, reminiscent of that observed in [23]. As a consequence, we interrogated the possibility that FHL2 is also part of the cardiac dyad complex. Our immunofluorescence analysis in adult mouse hearts, however, did not show distinct colocalisation of FHL2 with RyR2 or JPH2. This suggests that FHL2 might not be associated with cardiac dyads and the interaction with CMYA5 might occur at a different subcellular structure within cardiac myocytes.

A physiological relationship between FHL2 and CMYA5 was demonstrated by immunohistochemical and immunofluorescence analysis obtained from WT and *Fhl2* KO hearts. This revealed that FHL2 might

impact the subcellular distribution of CMYA5. Thereby, in *Fhl2* KO heart sections, CMYA5 immunohistochemical staining displayed perinuclear accumulation. This has been reported before representing a predominant subcellular location of CMYA5 in neonatal mouse cardiac myocytes [39]. There, CMYA5 was shown to interact with desmin close to endoplasmic reticulum membrane structures, as well as to the endoplasmic reticulum-Golgi compartment [39]. In adult cardiac myocytes and hearts, perinuclear localisation of CMYA5 was still detectable but diminished, and instead, CMYA5 was reported to distribute to other cardiac myocyte regions such as sarcoplasmic reticulum, costameres and intercalated discs [23,39]. Immunofluorescence analysis of *Fhl2* KO hearts revealed redistribution of CMYA5 to the intercalated disc region. This result was corroborated in sections from *Myhpc3* KI mouse hearts, which display reduced FHL2 expression levels [4], and in which CMYA5 also accumulated to the intercalated disc regions. In essence, this suggests that FHL2 might regulate CMYA5 localisation at certain cellular subcompartments in adult cardiac myocytes.

Our study additionally showed that FHL2 binds to the N- and C-terminal regions of CMYA5, of which aa206–265, aa336–365, aa3836–3865 and 3886–3935 served as the putative binding interface with FHL2. To our knowledge, FHL2 is the second protein interaction partner of the CMYA5 N-terminal region, the other being the cAMP-dependent protein kinase (PKA), an interaction inferred by the ability of PKA to *in vitro* phosphorylate CMYA5 at a sequence encompassing aa138–158 [38]. Most other known CMYA5 interactions are mediated by its C-terminal region, which contains a TRIM-like motif. CMYA5 associates with cytoskeletal and sarcomeric proteins, such as desmin [39], dystrophin [19], dysbindin [18], α -actinin [24] and M-band titin [40], as well as RyR2 [23]. CMYA5 is, therefore, considered as a part of the cytoskeletal network that maintains myocyte cytoarchitecture [42]. The C-terminal region of CMYA5 is also an anchoring point for PKA and calcineurin [38,43]. Because of its property to interact with the PKA regulatory subunit II α , CMYA5 represents a muscle-specific A-kinase-anchoring protein (AKAP) [38].

Comparison of the interaction interface between CMYA5 with FHL2 and the other CMYA5 interaction partners reveals that FHL2 binds to the CMYA5 regions that also interact with α -actinin [24], M-band titin [40], dystrophin [19], calcineurin [43] and other CMYA5 molecules involved in self-association [18]. It is then feasible that FHL2 contributes to the regulation of the spectrum of interactions of CMYA5. For

example, FHL2 and CMYA5 have as a common protein interaction partner the phosphatase calcineurin [11,43]. The FHL2–calcineurin interaction was investigated in cardiac myocytes in which FHL2 inhibited the calcineurin–dependent pathological cardiac myocyte growth [11]. Like FHL2, CMYA5 also attenuated calcineurin activity [43]. Experiments in transgenic mice with constitutively active calcineurin showed that animals overexpressing the CMYA5 C-terminal TRIM-like domain had attenuated skeletal muscle fibre conversion, compared to animals without CMYA5 TRIM-like domain overexpression. This was attributed to reduced gene transcription mediated by the nuclear factor of activated T cells, a transcription factor regulated by calcineurin [43]. The interaction of CMYA5 to calcineurin was mapped to a sequence immediately upstream of the BBC domain, the first FNIII domain and the SPRY domain [43]. Because part of the SPRY domain also binds to FHL2, it is tempting to speculate that the two scaffold proteins, FHL2 and CMYA5, cooperate to limit calcineurin activity in striated myocytes. However, this hypothesis, together with the potential impact of the FHL2–CMYA5 interaction on other FHL2- or CMYA5-binding partners, was not explored in the present study and, thus, merits further investigation in the future.

To study the significance of the FHL2–CMYA5 interaction for cardiac myocyte function, we exposed cells to peptides originating from the binding interface of the two proteins corresponding to the second FNIII domain of CMYA5, with the scope to modulate the interaction. Such an approach has been employed before to investigate interactions of PKA with other AKAP proteins and resulted in useful tools to manipulate PKA signalling with therapeutic prospects [44]. *In vitro* experiments suggested that the FNIII peptide did not affect the binding of FHL2 to V5/His₆-CMYA5_(3695–3906). However, the protein to peptide stoichiometry and the settings of this *in vitro* experiment might not exactly recapitulate the effect of the peptide on the FHL2–CMYA5 interaction in the native NRVM environment. Here, peptide administration had an impact on the development of hypertrophy. Attempts to visualise the effect of the peptide on the FHL2–CMYA5 interaction in cells with the PLA assay were, however, fruitless due to technical issues and this is an obvious limitation of the current work. It is also important to note that it remains unclear whether application of just the FNIII peptide would be sufficient to completely dissociate FHL2 from CMYA5 in cardiac myocytes. This is because FHL2 additionally interacted with the N-terminal region of CMYA5 and it could potentially also associate with the CMYA5

region encompassing aa2501–3000, which was not possible to test in our study. Nevertheless, our results showed that exposure to the FNIII peptide exerted functional consequences since it increased cardiac myocyte cell area at basal conditions and attenuated the increase in the PE-induced hypertrophic growth. Since FHL2 is not the only protein that interacts with the second CMYA5 FNIII domain, and α -actinin [24], dystrophin [19] and other self-associating CMYA5 molecules [18] also bind to that CMYA5 region, it cannot be excluded that the observed effect of the FNIII peptide arose from an impact on the association of CMYA5 with multiple binding partners. Of these interactions, however, it is less probable that the FNIII peptide influenced α -actinin binding, because this interaction extended beyond the CMYA5 TRIM-like domain and a CMYA5 C-terminus deletion mutant devoid of the FNIII domains could still associate with α -actinin [24].

Lastly, we hypothesised that the relationship of FHL2 with CMYA5 was not only physical and, because FHL2 also serves as a transcription factor coregulator [29], changes in FHL2 expression could affect CMYA5 transcription. Our observations that heterologous *Fhl2* overexpression in NRVM enhanced *Cmya5* gene expression and that lower abundance of FHL2 in *Mybpc3* KI hearts correlated with reduced *Cmya5* mRNA levels supported this assumption. In myocytes, *Cmya5* gene expression is driven by the myocyte enhancer factor 2A (MEF2A) and cAMP-response element-binding protein (CREB) transcription factors [19,24,45]. It is unlikely that FHL2 could exert its effect on *Cmya5* transcription through MEF2A, because previous studies by us and others showed that MEF2-dependent transcription was not affected by changes in FHL2 expression [8,9]. On the other hand, FHL2 is a co-activator of CREB transcriptional activity [36,46] and, subsequently, it is possible that FHL2 could impact on *Cmya5* gene expression through this transcription factor. Furthermore, our results verified previous data by Nakagami *et al.* [28] that PE induces an increase in *Cmya5* expression in NRVM. The fact that FHL2 overexpression did not further increase CMYA5 mRNA levels in response to PE could indicate that the transcriptional machinery that induces *Cmya5* expression was maximally activated by FHL2 overexpression.

Reduction in *Cmya5* transcript levels has also been reported recently in a *Mybpc3*-null mouse model of HCM [47]. This suggests that, at least in cardiomyopathy associated with *Mybpc3* mutations, which account for approximately 40–50% of inherited HCM [48], low CMYA5 abundance might be a common feature.

However, changes in *CMYA5* gene expression levels do not follow the same pattern in different types of heart-related disease. For example, *CMYA5* mRNA levels were higher in atrial samples from patients with atrial fibrillation or mitral regurgitation compared to healthy control samples [49] and the same was observed for *FHL2* mRNA levels in an independent cohort of patients with atrial fibrillation [50]. *Cmya5* and *Fhl2* mRNA levels were lower in mouse left ventricle samples 2 days postmyocardial infarction than in sham-operated animals, but no changes were detected in samples taken 2 weeks or 2 months after surgery [51]. Interestingly, different heart compartments could also reveal distinct regional changes in *Cmya5* gene expression following a disease-inducing intervention. Knyazeva *et al.* [52] used a rodent model of pressure overload-induced heart disease and observed that *Cmya5* mRNA levels declined in left ventricular samples 10 weeks following transverse aortic constriction (TAC), whereas the *Cmya5* expression increased in right ventricular samples and remained unchanged in interventricular septum samples. In the same study, *Fhl2* mRNA levels were not significantly altered, as it has also been shown previously in mice after TAC intervention [32]. Furthermore, in our work, inherent loss of FHL2 did not affect gene expression of *Cmya5* but only its localisation. Therefore, our overall mRNA data analysis and the above-mentioned studies reveal some association between FHL2 and CMYA5 levels without, however, confirming if FHL2 directly regulates *Cmya5* transcription. Thus, more detailed investigations are needed to interrogate how and under what conditions FHL2 modulates CMYA5 functions.

To conclude, our study demonstrated that CMYA5 is a novel interaction partner for FHL2 in cardiac myocytes and, that FHL2 is required for subcellular compartmentation of CMYA5 in the heart. The physiological impact of the FHL2–CMYA5 interaction may also relate to the regulation of cardiac myocyte growth, important for the development of heart disease.

Materials and methods

Materials

The Champion™ pET151 Directional TOPO® expression kit with One Shot® BL21 Star™ (DE3) chemically competent *Escherichia coli* cells (#K15101), High-Capacity cDNA Reverse Transcription kit (#4368814), Maxima™ SYBR™ Green/ROX 2x qPCR Master Mix (#K0221), Phusion Hot Start II DNA polymerase (#F549L), isopropyl- β -thiogalactopyranoside (IPTG), cell culture media, fetal calf

serum (FCS; #10270106), horse serum (HS; #26050088), penicillin/streptomycin (#15140122), TRIzol™, TurboFect™ (#R0531), goat anti-mouse Alexa Fluor™ 488 (#A11029), goat anti-mouse Alexa Fluor™ 647 (#A21236), DyLight™ 633-labelled phalloidin (#21840), Alexa Fluor™ 488-labelled wheat germ agglutinin (WGA; #W11261) and mouse anti-V5 tag (#460705) were from ThermoFischer Scientific (Waltham, MA, USA). The High Pure PCR Product Purification kit (#11732668001) and cOmplete™ protease inhibitors (#11697498001) were from Roche Diagnostics (Risch-Rotkreuz, Switzerland). The mouse monoclonal anti- α -actinin (#A7811) and anti-FLAG (#F3165) antibodies, the rabbit anti-RyR2 (#HPA020028) antibody, as well as anti-FLAG M2 agarose (#A2220) were from Sigma-Aldrich (Taufkirchen, Germany). Mouse monoclonal anti-FHL2 antibody was from Medical and Biological Laboratories (#K0055-3; Nagoya, Japan) and anti-glyceraldehyde-3-phosphate dehydrogenase (GAPDH) antibody from HyTest (#5G4; Turku, Finland). The mouse anti-connexin 43 antibody as from BD Transduction Laboratories (#610061; San Jose, CA, USA). Mouse anti-GST (#sc-138) and rabbit anti-JPH2 (#scH-250) antibodies were from Santa Cruz Biotechnologies (#sc-138; Dallas, TX, USA). The mouse anti-dystrophin antibody was from Merck Millipore (#MAB1645; Darmstadt, Germany). The rabbit anti-CMYA5 antibody (des122) has been described previously [18]. Ni/NTA agarose was from Qiagen (#30210; Venlo, The Netherlands). The goat anti-rabbit DyLight™ 550 antibody was from Abcam (#ab96884; Cambridge, UK). Paraformaldehyde (PFA) was from Agar Scientific (#R1026; Essex, UK). Tissue-Tek® O.C.T. was from Sakura Finetek Germany GmbH (#4583; Staufen, Germany). PE (#6126), 4',6-diamidin-2-phenylindol (DAPI; #32670) and all other standard chemicals were from Sigma-Aldrich (Taufkirchen, Germany). Glutathione-sepharose 4B beads (#17-0756-01), polyvinylidene fluoride (PVDF) membrane (#10600023), horseradish peroxidase (HRP)-linked sheep anti-mouse (#NA9310V) and donkey anti-rabbit (NA9340V) HRP secondary antibodies, enhanced chemiluminescence (ECL) kit (#RPN2106) and Amesham Hyperfilm™ ECL (#28906837) were from GE Healthcare (Buckinghamshire, UK). The adenovirus to express FLAG-tagged mouse FHL2 (Ad5:FLAG-*Fhl2*) was from Seven Hills Bioreagents (#JMAd-93; Cincinnati, OH, USA) and amplified in-house. The peptides corresponding to the second FNIII and the SPRY domains of CMYA5 (see below for details) were synthesised by JPT Peptide Technologies GmbH (Berlin, Germany).

Cloning and expression of recombinant proteins

Directional cloning of human CMYA5 was performed using the Champion™ pET151 Directional TOPO® expression kit (ThermoFischer Scientific) and resulting recombinant proteins are N-terminally His₆- and V5-tagged. For

this purpose, cDNA from human nonfailing heart was generated using the High-Capacity cDNA Reverse Transcription kit according to the manufacturer's instructions. The human myocardial sample was obtained by a procedure approved by the local ethics committee (Ethics Committee of the Medical Association of Hamburg 532/116/9.71991) and according to the Declaration of Helsinki. Patient data were handled anonymously, and no material was used or included without that written informed consent was obtained. The cDNA was afterwards used to amplify eight nonoverlapping *CMYA5* moieties using the following primers:

CMYA5_(1–500): CACCATGGCGAGCCGCGATAGCAAC (forward), TCACATTAGAGGTTTCAGAAAGAGA (reverse).

CMYA5_(501–1000): CACCTTAGAAGAACCAGAGAAA-GAAGAA (forward), TCATGGAGAGAACAGTTCCGCTTC (reverse).

CMYA5_(1001–1500): CACCGACTCAGCATCACAAGTTTCAATC (forward), TCAAGAAAATAAAAGATCTTGT TTGTC (reverse).

CMYA5_(1501–2000): CACCACAGTCTGTGACTCTGAA CGTTTG (forward), TCATACATTTCCAGCTAGGACT AAAGAC (reverse).

CMYA5_(2001–2500): CACCGAGAGAAACATAGCAGA GGGGAAG (forward), TCAAGATCCAAGTGTAATTT GTGTCTTC (reverse).

CMYA5_(2501–3000): CACCAGATCTACTGAACTGAAA GAATC (forward), TCAACAAGCAACTGTTTCACTAT-CATC (reverse).

CMYA5_(3001–3500): CACCATAAAACATTAAGAG-CAGG (forward), TCATGCCTTTTCAGTTACTACCTC (reverse).

CMYA5_(3501–4069): CACCCAAAAGAGCTGAAAAA GTCCAG (forward), TCACTTGTGCCTTACAGAATC CG (reverse).

CMYA5_(3695–3906): CACCATGGCGAGCCGCGATAG-CAAC (forward), TCACATTAGAGGTTTCAGAAAGAGA (reverse).

Amplification was performed by PCR using the Phusion Hot Start II DNA polymerase. The PCR cycling protocol included a 30-s initial denaturation at 98 °C and 35 cycles of denaturation at 98 °C (5 s), annealing at 63 °C (30 s) and extension at 72 °C (80 s). This was followed by a 7-min final extension at 72 °C and a hold at 4 °C. The PCR products were purified using the Roche High Pure Product Purification kit. 2 µL of purified PCR product were then used for directional cloning in the Champion™ pET151 vector. One Shot TOP10 cells were transformed with the recombinant vector and after amplification of positive clones, plasmid DNA was isolated and successful cloning was verified by sequencing.

Recombinant CMYA5 protein moieties were then expressed in One Shot® BL21 Star™ (DE3) chemically competent *E. coli* cells after induction with 5 mmol·L⁻¹ IPTG

for 5 h at 30 °C. For protein purification, cells were pelleted by centrifugation at 4 °C for 20 min at 4000 g in a Beckman J2-21 centrifuge, washed once with ice cold PBS and lysed with 10 mL lysis buffer (in mmol·L⁻¹: 50 NaH₂PO₄·H₂O, 300 NaCl, 10 imidazole, pH 8.0). Following centrifugation as above, the supernatant (S/N) was collected and sonicated five times for 25 s, with 20 s intervals, in a Sonopuls HD 2200 ultrasonic homogeniser (38% power; Bandelin, Berlin, Germany). The sonicated lysate was further cleared by centrifugation at 4 °C for 35 min at 10 000 g. The cleared lysate was then added on 1 mL Ni/NTA agarose in a polypropylene column and incubated for 1 h at 4 °C on a spinning wheel to allow binding of the His₆-tagged CMYA5 moieties. The lysate was then allowed to flow through by gravity and the Ni/NTA agarose column was washed twice at 4 °C with 10 mL wash buffer (in mmol·L⁻¹: 50 NaH₂PO₄·H₂O, 300 NaCl, 20 imidazole, pH 8.0). Recombinant proteins were eluted with 4 mL elution buffer (in mmol·L⁻¹: 50 NaH₂PO₄·H₂O, 300 NaCl, 250 imidazole, pH 8.0) and dialysed overnight in 1.5 L dialysis buffer (in mmol·L⁻¹: 50 Tris pH 8.1, 1 EDTA, 1 DTT supplemented with 0.1% (v/v) Triton X-100) under gentle stirring at 4 °C. Protein concentration was determined by Bradford assay and proteins were concentrated using the Centricon® YM-30 centrifugal devices (Merck Millipore, Burlington, MA, USA) according to the manufacturer's instructions.

Expression and purification of recombinant human GST-FHL2 and GST has been described previously [9].

***In vitro* pull-down assay**

In vitro GST pull-down assays were conducted by initially incubating 200 pmol GST-FHL2 or, as control, 200 pmol GST with 50 µL glutathione-sepharose 4B beads in 500 µL assay buffer (30 mmol·L⁻¹ Tris pH 7.4, 15 mmol·L⁻¹ MgCl₂, 1 mmol·L⁻¹ DTT, 1% (v/v) Triton X-100). Incubation took place under rotation at 4 °C and for 1 h. Subsequently, 400 pmol recombinant His₆-V5-CMYA5 proteins were added to the tubes and samples were incubated for another 2 h at 4 °C under rotation. As additional control, His₆-V5-CMYA5 proteins were incubated only with glutathione-sepharose 4B beads. The mixtures were then centrifuged at 1500 g (4 °C, 90 s), the S/Ns (unbound proteins) collected, and the pellets were washed three times with 500 µL assay buffer (1500 g, 4 °C, 90 s). Precipitated proteins were extracted by mixing the bead pellets with 70 µL 3× Laemmli sample buffer (187.5 mmol·L⁻¹ Tris pH 6.8, 6% (w/v) SDS, 9% (v/v) β-mercaptoethanol, 30% (v/v) glycerol and 0.03% (w/v) bromophenol blue).

FLAG-FHL2 immunoprecipitation

HEK293T cells were maintained in Dulbecco's Modified Eagle Medium (DMEM) supplemented with 10% (v/v)

FCS, 2 mmol·L⁻¹ glutamine and 100 IU·mL⁻¹ penicillin/streptomycin in an incubator at 37 °C and with 7% (v/v) CO₂ atmosphere. HEK293T cells were seeded at a density of 200 000/well in six-well plates and 24 h later were transfected with 1 µg plasmid expressing FLAG-tagged FHL2 using Turbofect™ according to the manufacturer's instructions. Cells that were not transfected were used as control. The following day, cells were lysed in 200 µL per well IP buffer (in mmol·L⁻¹: 50 Tris pH 7.4, 150 NaCl, supplemented with 1% (v/v) Triton X-100 and cOmplete™ protease inhibitors). Three wells per condition were pooled together and 50 µL lysate were collected as crude lysate and mixed with 25 µL 3× Laemmli sample buffer. The rest lysate was incubated on ice for 30 min and then centrifuged at 4 °C and at 12 000 g for 10 min. The resulting S/N1 was collected and of this 50 µL were mixed with 25 µL 3× Laemmli sample buffer. 400 µL of the rest S/N1 were mixed with 30 µL anti-FLAG M2 agarose (Sigma-Aldrich) and incubated for 4 h at 4 °C under rotation. This was followed by centrifugation at 4 °C and at 5000 g for 30 s, after which the S/N (S/N2) was collected and the beads with immunoprecipitated FLAG-FHL2 were washed once with 300 µL IP buffer. The beads were then incubated at 4 °C for 2 h under rotation with 100 pmol His₆-V5-CMYA5_(3695–3906) in 500 µL IP buffer. After that, the tubes were centrifuged as mentioned before, the S/N collected (S/N3) and beads were washed four times with IP buffer. Immunoprecipitated and bound proteins were finally eluted by adding 70 µL 2× Laemmli sample buffer to the beads.

For experiments in the presence of peptides (please see below the section 'ARVM and NRVM treatments'), immunoprecipitated FLAG-FHL2 was aliquoted in four tubes and incubated for 5 h at 4 °C with 10 pmol His₆-V5-CMYA5_(3695–3906) in the presence of either FNIII peptide (10 nmol), SPRY peptide (10 nmol), a combination of the FNIII (5 nmol) and SPRY (5 nmol) peptides or DMSO (1 µL) as control. The final volume of the reaction mixture was 300 µL.

Peptide array assay

A peptide array assay was performed as described in [53,54] with some modifications. The human CMYA5 moieties representing aa1–500 and aa3501–4069 were synthesised as overlapping 25-aa-long peptides with 5-aa shifts using the automated multiple peptide synthesiser MultiPep Celluspot (INTAVIS Bioanalytical Instruments AG, Cologne, Germany). The peptides were synthesised on cellulose discs employing fluorenylmethyloxycarbonyl (Fmoc) chemistry and at a synthesis scale of 2 µmol. Following peptide synthesis, the cellulose discs were placed in 96-well plates and Fmoc side chains were removed from the peptides by incubation for 1 h, at room temperature, with 150 µL cleavage solution containing 80% (v/v) trifluoroacetic acid (TFA), 3% (v/v) triisopropylsilyl ether

(TIPS) and 12% (v/v) dichloromethane. After aspiration of that solution, 250 µL cellulose solvation solution (88.5% (v/v) TFA, 4% (v/v) trifluoromethanesulfonic acid, 2.5% (v/v) TIPS) was added to each well and the plates were incubated overnight at room temperature. 750 µL ice-cold methyl tert-butyl ether was pipetted into each well and the plates were inverted ten times, then incubated for 1 h at –20 °C and span at 2000 g for 20 min at 4 °C. The ether was tipped off and the procedure was repeated without incubation at –20 °C. The plates were placed in a fume hood for 15 min, then 300 µL DMSO were added to each well and the plates were left open for 2 h. To spot the peptides on coated slides, 30 µL peptide solution was mixed with 10 µL SSC buffer (150 mmol·L⁻¹ NaCl, 15 mmol·L⁻¹ trisodium citrate pH 7.0) and transferred into a 384-well plate. Spotting was done automatically with the use of a Slide Spotting Robot (INTAVIS Bioanalytical Instruments AG) according to the manufacturer's instructions. The slides were hydrated in TBS-T (20 µmol·L⁻¹ Tris pH 7.6, 137 µmol·L⁻¹ NaCl, 0.01% (v/v) Tween-20), nonspecific binding sites were blocked for 2 h with 3 mL 5% (w/v) BSA in TBS-T, rinsed again in TBS-T and, finally, incubated overnight with 0.1 µmol recombinant GST-FHL2 or GST diluted in 2.5 mL 0.5% (w/v) BSA in TBS-T, at 4 °C and under shaking conditions. The next day, the slides were washed three times for 10 min with TBS-T and then incubated overnight at 4 °C with an anti-GST antibody diluted in 1% (w/v) BSA in TBS-T. This was ensued by three 5-min washes with TBS-T and incubation for 1 h with secondary antibody solution in 1% (w/v) BSA in TBS-T. After three more washes, the slides were incubated with ECL solution and signals were developed on a photosensitive film.

Animals

All experiments involving animals complied with the guidelines for the use and care of laboratory animals published by the National Institutes of Health (Bethesda MD, USA; Publication No. 85-23, revised 1985). The experimental procedures were in accordance with the German Law for the Protection of Animals and accepted by the local authorities (Animal Care and Use Committee: Behörde für Gesundheit und Verbraucherschutz, Ministry of Science and Public Health of the City State of Hamburg, Germany). Approval by the local authorities for breeding and housing of the *Mybpc3* c.772G>A KI (*Mybpc3* KI) mice occurs under the Zuchtantrag Nr. N098/2020 'Zucht und Haltung belasteter genetisch veränderter Mäuse zur Untersuchung der Pathomechanismen bei Dilatativer und Hypertropher Kardiomyopathie' and the University Medical Center Hamburg-Eppendorf, Germany. The *Mybpc3* KI mouse model of HCM has been described previously [55]. The *Fhl2*-targeted KO mice have been described in [13] and breeding and housing of these animals was approved by

the local authorities (Landesamt für Natur, Umwelt und Verbraucherschutz Nordrhein-Westfalen, Germany, AZ 8.87-51.05.20.10.147). ARVM were isolated from male Wistar rats (weighing 150–200 g; Charles River Laboratories, Sulzfeld, Germany). NRVM were isolated from 0–3-day-old Wistar rats.

Adult and neonatal rat ventricular myocyte preparation

ARVM isolation and culture was performed as described in [56] and [57]. NRVM were isolated from the hearts of rat neonates by a fractionated DNase/trypsin protocol described in [58]. Following cell isolation, the heart cell mixture was plated on a cell culture dish and incubated for 90 min in a humid incubator at 37 °C and 7% (v/v) CO₂. During this step, the nonmyocytes can attach to the dish, whilst the myocytes remain suspended at the culture medium. The myocytes were then collected and plated with plating medium (% v/v: 68 DMEM with GlutaMax™ (ThermoFischer Scientific, Waltham, MA, USA), 17 M199, 10 FCS, 5 HS and supplemented with 1% penicillin/streptomycin) on cell culture dishes previously coated with 1% (v/v) gelatin (Sigma-Aldrich; Taufkirchen, Germany). The next day, the medium was changed to maintenance medium (MM; % v/v: 80 DMEM with GlutaMax™, 20 M199) with or without 1% (v/v) FCS, depending on the experiment, and experimental procedures were performed as described in subsequent sections.

ARVM and NRVM treatments

Two peptides corresponding to the FNIII (YTLEYCRQH-SPEGEGLRSFSGIKGL) and the SPRY (LQISSNGT-VISFERRRLTEIPSVL) domains of rat CMYA5 protein sequence were synthesised by JPT Peptide Technologies GmbH (Berlin, Germany). The peptides were conjugated at the N-terminus with a myristoyl moiety and at the C-terminus with 5(6)-FAM. In preliminary experiments, NRVM cultured in 35-mm dishes were incubated with 10 μmol·L⁻¹ of either peptide or an equivalent volume (10 μL) of vehicle (DMSO). Eight hours later cells were fixed for immunofluorescence staining as described later.

To test the impact of the FNIII peptide on the PE-induced hypertrophy, NRVM were plated at a density of 4 × 10⁵ cells per 35-mm dish, incubated for 18–24 h in MM +1% (v/v) FCS and then medium was changed to simple MM. Cells were then treated with 5 μmol/L FNIII peptide or an equivalent volume of vehicle (DMSO; 5 μL). 8 h later, cells from each condition were treated with 10 μmol·L⁻¹ PE or vehicle H₂O (2 μL). After 24 h, the peptide was reapplied by removing 500 μL of cell culture medium from the cells and adding 500 μL fresh MM containing 20 μmol·L⁻¹ FNIII peptide or DMSO, with or without 10 μmol·L⁻¹ PE. The cumulative FNIII peptide

concentration in the end of the experiment was 8.75 μmol·L⁻¹, whilst the PE concentration remained 10 μmol·L⁻¹. Cells were then cultured for another 24 h, after which time point, they were fixed and processed for cell area analysis by immunofluorescence.

For experiments involving FHL2 overexpression, NRVM were either plated at a density of 2.2 × 10⁶ cells in 60-mm dishes for RNA extraction or at a density of 4 × 10⁵ cells per 35-mm dish for immunoblotting or for cell area measurements by immunofluorescence. Plating medium was changed to MM (without FCS) containing Ad5:FLAG-*Fhl2*. Control cells were left untransduced. Three hours later cells were exposed to 10 μmol·L⁻¹ PE or vehicle (H₂O) and treatment lasted 48 h, after which time NRVM were harvested for RNA extraction or fixed for immunofluorescence. For immunoblotting, cells were harvested in 150 μL 1 × Laemmli sample buffer.

Immunofluorescence

Immunofluorescence in ARVM and NRVM was performed as described previously [59]. Briefly, myocytes were washed twice with PBS and then fixed in 4% (v/v) PFA for 10 min at room temperature. Following this, cells were washed three times for 5 min with PBS, permeabilised for 5 min with 0.2% (v/v) Triton X-100 in PBS, washed again with PBS and then incubated with 5% (v/v) NGS in BSA/gold buffer (in mmol·L⁻¹: 20 Tris pH 7.5, 155 NaCl, 2 EGTA, 2 MgCl₂, supplemented with 1% (w/v) BSA) in a humid chamber for 20 min, at room temperature and under orbital shaking, to block nonspecific binding sites. After three 5-min washes with PBS, cells were incubated overnight with primary antibodies diluted in BSA/gold buffer (anti-FHL2, 1 : 100; anti-CMYA5, 1 : 100) in a humid chamber, at 4 °C and under orbital shaking. Cells were then washed three times for 5 min with PBS and incubated for 3 h with a mixture of DAPI (1 : 100), goat anti-rabbit DyLight™ 550 (1 : 100) and goat anti-mouse Alexa Fluor™ 488 (1 : 100) secondary antibodies in BSA/gold buffer, at room temperature and under orbital shaking. Subsequently, cells were washed three times for 5 min with PBS and mounting medium (30 mmol·L⁻¹ Tris pH 9.5, 235.6 mmol·L⁻¹ *n*-propyl gallate, 70% (v/v) glycerol) and a coverslip were added and sealed with transparent nail varnish. For cell area measurements, NRVM were stained with anti-α-actinin antibody (1 : 100) and Alexa Fluor™ 633 phalloidin (1 : 100), the latter applied along with the secondary antibody. Observation was performed in a blinded fashion.

For immunofluorescence experiments in heart sections from WT, *Fhl2* KO or *Mybpc3* C772G>A KI mice, hearts were excised from the body, washed twice in PBS to remove excess blood and immediately frozen in cryotubes in liquid nitrogen. Hearts were then stored at -80 °C until further processing. Frozen hearts were embedded in Tissue

Tek O.C.TTM Compound and sections with a thickness of 10 μm were prepared by using a cryostat. The sections were transferred to Super-Frost Plus adhesion microscope slides (R. Langenbrinck GmbH, Emmendingen, Germany), left to dry overnight at room temperature and then fixed for 5 min at $-20\text{ }^{\circ}\text{C}$ with prechilled acetone. This was followed by rehydration of the sections in PBS for 5 min at room temperature and incubation with 5% (v/v) NGS in BSA/gold buffer for 20 min, at room temperature and in a humid chamber. Sections were then washed three times for 5 min with PBS and incubated for 2 h under orbital shaking with antibodies against FHL2 (1 : 100), CMYA5 (1 : 100), connexin 43 (1 : 100), RyR2 (1 : 300) or JPH2 (1 : 100) diluted in BSA/gold buffer. Subsequently, sections were washed with PBS and incubated for 1 h at room temperature with a mixture of DAPI, Alexa FluorTM 488 WGA, anti-rabbit DyLightTM 550 and anti-mouse Alexa FluorTM 647 secondary antibodies. Following three washes with PBS, mounting medium was added and sections sealed with a coverslip.

Samples were finally observed under a LSM 800 Airyscan confocal microscope (Carl Zeiss Microscopy Deutschland GmbH, Oberkochen, Germany). Image extraction and processing was performed by using either the ZEN 2012 software (Blue edition, version 1.1.2.0; Carl Zeiss Microscopy Deutschland GmbH) or ImageJ (from the Fiji image processing package; [60]). NRVM cell area was measured using the IMAGEJ software.

Proximity ligation assay

Proximity ligation assay was performed using the DuolinkTM In Situ Orange Starter Mouse/Rabbit kit (Sigma-Aldrich; Taufkirchen, Germany) employing a custom protocol as described previously [59] with some modifications. The PLA probes, buffers A and B, the ligase and polymerase along with their dilution buffers and mounting medium with DAPI were included in the kit. Briefly, ARVM were fixed and processed as described in the 'Immunofluorescence section'. Cells were stained overnight with anti-FHL2 and anti-CMYA5 antibodies, alone or in combination. After washing two times for 10 min with PBS, cells were incubated for 1 h with the PLA probes diluted in BSA/gold buffer, at $37\text{ }^{\circ}\text{C}$ and in a humid chamber. This was followed by two 5-min washes with buffer A and incubation with the ligase mix (30 min, $37\text{ }^{\circ}\text{C}$, humid chamber). After two 2-min washes with buffer A, cells were incubated with the polymerase mix (100 min, $37\text{ }^{\circ}\text{C}$, humid chamber), washed two times for 10 min with buffer B and once for 2 min with 1 : 100 diluted buffer B. Mounting medium with DAPI was then added on the cells which were finally sealed with a coverslip. Samples were observed under an Eclipse Ti inverted microscope (Nikon Instruments Europe BV, Amsterdam, The Netherlands) and the accompanying NIS-Elements software v4.20 was used to acquire and

process images. A brightfield image was also acquired to define the myocyte cell size. For the digital count of PLA signals, a signal intensity threshold was defined automatically by the software. Results were then expressed as PLA object counts $\cdot\mu\text{m}^{-2}$. All images were acquired under identical laser settings and processed in an identical manner.

Immunohistochemical analysis of WT and *Fhl2*-targeted KO mouse hearts

Tissues were fixed in 4% buffered formalin, dehydrated, and embedded in paraffin. Sections were cut at $2\text{ }\mu\text{m}$ and subjected to H&E staining according to standard procedures or processed for immunohistochemical staining as follows: After dewaxing and inactivation of endogenous peroxidases (PBS/3% hydrogen peroxide), antibody-specific antigen retrieval was performed using the Ventana Benchmark XT machine (Ventana, Tuscon, AZ, USA). Sections were incubated with the anti-CMYA5 (1 : 100), anti-FHL2 (1 : 100) or anti-dystrophin (1 : 100) antibody for 1 h. Anti-rabbit or anti-mouse Histofine Simple Stain MAX PO Universal immunoperoxidase polymer (Nichirei Biosciences, Wedel, Germany) were used as secondary antibodies. Detection of secondary antibodies and counter staining was performed with an ultraview universal DAB detection kit from Ventana. Stainings were evaluated by an experienced pathologist in a blinded fashion and representative images were taken with a Leica DMD108 digital microscope. Cross-sectional area of cardiac myocytes was measured using ImageJ software.

Heart tissue fractionation

Hearts were pulverised under liquid nitrogen and tissue was homogenised in a buffer consisting of $100\text{ mmol}\cdot\text{L}^{-1}$ Tris pH 7.4, 1% (v/v) Triton X-100 and cOmpleteTM protease inhibitors to generate 10% (w/v) homogenates. The homogenates were incubated for 10 min on ice and then centrifuged at $15\text{ }000\text{ g}$, for 10 min and at $4\text{ }^{\circ}\text{C}$. The S/Ns, which comprise the detergent-soluble fraction, were collected and mixed with $3\times$ Laemmli sample buffer (volume added: $1/3$ the volume of the S/N for each sample). The pellets remaining after the centrifugation comprise the detergent-insoluble fraction of each sample and were resuspended in a volume of $3\times$ Laemmli sample buffer equal to the final volume of the respective S/N. Samples were boiled at $95\text{ }^{\circ}\text{C}$ for 5 min and stored at $-20\text{ }^{\circ}\text{C}$ until used for immunoblot analysis.

Immunoblot analysis

Immunoblot analysis was performed as previously described [59]. Following SDS-polyacrylamide gel electrophoresis, proteins were transferred onto PVDF membranes

and then nonspecific binding sites were blocked with 10% (w/v) nonfat milk in TBS-T buffer. Membranes were then incubated overnight at 4 °C with anti-V5 (1 : 5000), anti-GST (1 : 1000), anti-FHL2 (1 : 1000), anti-FLAG (1 : 1000), anti-CMYA5 (1 : 1000), anti- α -actinin (1 : 1000) or anti-GAPDH (1 : 5000) primary antibodies, depending on the experiment, diluted in 1% (w/v) milk in TBS-T. Subsequently, membranes were washed four times for 15 min with TBS-T and incubated with HRP-linked sheep anti-mouse secondary antibody (1 : 2000) for 1 h, at room temperature. Following four more washes with TBS-T, membranes were incubated with ECL reagents and signals were acquired after exposing the membranes to photosensitive film. For some blots, signal acquisition took place using the ChemiDoc Imaging System (Bio-Rad, Hercules, CA, USA) and images were extracted with the accompanying Image Lab v5.2.1 software (Bio-Rad).

Gene expression analysis

For gene expression analysis, RNA was extracted from 30 to 50 mg of pulverised mouse heart tissue or 2.2×10^6 NRVM using 1 mL Trizol™ according to the manufacturer's instructions. Subsequently, cDNA was synthesised from 500 ng isolated RNA per sample using the High Capacity cDNA Reverse Transcription kit (ThermoFischer Scientific) and following the instructions of the kit's manual. Gene expression was analysed by real-time qPCR with reactions made up using the Maxima SYBR Green/ROX qPCR Master Mix (2 \times) and the following primers: *Cmya5* (rat): AGGGGAGAGCTCATGGTACA, TGTCCTACTCTCGGCGTTTAC; *Cmya5* (mouse): ACTGGAGCGTGAA-CAAGGAG, GCCATCACCCACACTTGGTA; *Fhl2* (mouse): CTTACAGCACGGGATGAGT, CCAGAGACAGGGAGCACTTC; *Gnas* (rat and mouse): CAAGGCTCTGTGGGAGGAT, CGAAGCAGGTCCTGGTCACT. qPCR was performed in a 7900HT ABI PRISM Sequence Detection System (Applied Biosystems, Foster City, CA, USA) and data were exported using the accompanying SDS v2.3 software (Applied Biosystems). Data were normalised to *Gnas* and are expressed as fold change over control as described in the respective figure legends.

Statistical analysis

Data were analysed using the GRAPHPAD PRISM v.6 software (GraphPad Software Inc., San Diego, CA, USA). The PLA data were compared by one-way ANOVA with Tukey's *post hoc* test. Statistical evaluation of mRNA expression and immunoblot analysis in mouse hearts was performed using two-tailed Student's *t*-test. Data from NRVM cell area measurements and mRNA expression were analysed by two-way ANOVA with Bonferroni's *post hoc* test. Sample numbers are given in the respective figure legends. Data

are given as mean \pm SD. A value of $P < 0.05$ was considered significant.

Acknowledgements

The project was supported by the Deutsche Stiftung für Herzforschung (grant F/40/17), the Deutsches Zentrum für Herz-Kreislauf Forschung and the Deutsche Forschungsgemeinschaft (DFG CU 53/5-1). J.R. was supported by a fellowship of the Studienstiftung des deutschen Volkes. Work in the Ehler laboratory is funded by the British Heart Foundation and by the Medical Research Council (MR/R017050/1). The funding sources had no involvement in the study design, collection, analysis and interpretation of data, writing of the manuscript or decision to submit the article for publication. We thank the Mouse Pathology core facility and the Vector Facility of the University Medical Center Hamburg-Eppendorf for their help with the immunohistochemical staining of mouse hearts and the adenovirus purification respectively. Open access funding enabled and organized by ProjektDEAL.

Conflict of interest

The authors declare no conflict of interest.

Author contributions

KS, JS, FF, FC, JR, NM, JF, KH and GB performed experiments; KS, JS and FF analysed data; SK. evaluated the immunohistochemical stainings; AP and JU provided technical support; EE, SS, LC, VW, DJB and GSB provided critical materials and expertise for the project; KS and FC designed experiments, obtained funding and wrote the manuscript; FC conceived and supervised the project. All authors have read and agreed to the submission of the manuscript.

References

- Lorenz K, Stathopoulou K, Schmid E, Eder P, Cuello F. Heart failure-specific changes in protein kinase signalling. *Pflugers Arch.* 2014;**466**:1151–62.
- Kadmas JL, Beckerle MC. The LIM domain: from the cytoskeleton to the nucleus. *Nat Rev Mol Cell Biol.* 2004;**5**:920–31.
- Bovill E, Westaby S, Crisp A, Jacobs S, Shaw T. Reduction of four-and-a-half LIM-protein 2 expression occurs in human left ventricular failure and leads to

- altered localization and reduced activity of metabolic enzymes. *J Thorac Cardiovasc Surg.* 2009;**137**:853–61.
- 4 Friedrich FW, Reischmann S, Schwalm A, Unger A, Ramanujam D, Munch J, et al. FHL2 expression and variants in hypertrophic cardiomyopathy. *Basic Res Cardiol.* 2014;**109**:451.
 - 5 Lal S, Nguyen L, Tezone R, Ponten F, Odeberg J, Li A, et al. Tissue microarray profiling in human heart failure. *Proteomics.* 2016;**16**:2319–26.
 - 6 Gao J, Collyer J, Wang M, Sun F, Xu F. Genetic dissection of hypertrophic cardiomyopathy with myocardial RNA-Seq. *Int J Mol Sci.* 2020;**21**:3040.
 - 7 Christodoulou DC, Wakimoto H, Onoue K, Eminaga S, Gorham JM, DePalma SR, et al. 5'RNA-Seq identifies *Fhl1* as a genetic modifier in cardiomyopathy. *J Clin Invest.* 2014;**124**:1364–70.
 - 8 Purcell NH, Darwis D, Bueno OF, Muller JM, Schule R, Molkenstein JD. Extracellular signal-regulated kinase 2 interacts with and is negatively regulated by the LIM-only protein FHL2 in cardiomyocytes. *Mol Cell Biol.* 2004;**24**:1081–95.
 - 9 Stathopoulou K, Cuello F, Candasamy AJ, Kemp EM, Ehler E, Haworth RS, et al. Four-and-a-half LIM domains proteins are novel regulators of the protein kinase D pathway in cardiac myocytes. *Biochem J.* 2014;**457**:451–61.
 - 10 Sun J, Yan G, Ren A, You B, Liao JK. FHL2/SLIM3 decreases cardiomyocyte survival by inhibitory interaction with sphingosine kinase-1. *Circ Res.* 2006;**99**:468–76.
 - 11 Hojaye V, Rothermel BA, Gillette TG, Hill JA. FHL2 binds calcineurin and represses pathological cardiac growth. *Mol Cell Biol.* 2012;**32**:4025–34.
 - 12 Lange S, Auerbach D, McLoughlin P, Perriard E, Schafer BW, Perriard JC, et al. Subcellular targeting of metabolic enzymes to titin in heart muscle may be mediated by DRAL/FHL-2. *J Cell Sci.* 2002;**115**:4925–36.
 - 13 Kong Y, Shelton JM, Rothermel B, Li X, Richardson JA, Bassel-Duby R, et al. Cardiac-specific LIM protein FHL2 modifies the hypertrophic response to β -adrenergic stimulation. *Circulation.* 2001;**103**:2731–8.
 - 14 McLoughlin P, Ehler E, Carlisle G, Licht JD, Schafer BW. The LIM-only protein DRAL/FHL2 interacts with and is a corepressor for the promyelocytic leukemia zinc finger protein. *J Biol Chem.* 2002;**277**:37045–53.
 - 15 Sarparanta J. Biology of myospryn: what's known? *J Muscle Res Cell Motil.* 2008;**29**:177–80.
 - 16 Tsoupri E, Capetanaki Y. Myospryn: a multifunctional desmin-associated protein. *Histochem Cell Biol.* 2013;**140**:55–63.
 - 17 Tkatchenko AV, Pietu G, Cros N, Gannoun-Zaki L, Auffray C, Leger JJ, et al. Identification of altered gene expression in skeletal muscles from Duchenne muscular dystrophy patients. *Neuromuscul Disord.* 2001;**11**:269–77.
 - 18 Benson MA, Tinsley CL, Blake DJ. Myospryn is a novel binding partner for dysbindin in muscle. *J Biol Chem.* 2004;**279**:10450–8.
 - 19 Reynolds JG, McCalmon SA, Donaghey JA, Naya FJ. Deregulated protein kinase A signaling and myospryn expression in muscular dystrophy. *J Biol Chem.* 2008;**283**:8070–4.
 - 20 Xu J, Li Z, Ren X, Dong M, Li J, Shi X, et al. Investigation of pathogenic genes in chinese sporadic hypertrophic cardiomyopathy patients by whole exome sequencing. *Sci Rep.* 2015;**5**:16609.
 - 21 Zhang R, Zhang H, Li M, Li H, Li Y, Valenzuela RK, et al. Genetic analysis of common variants in the *CMYA5* (cardiomyopathy-associated 5) gene with schizophrenia. *Prog Neuropsychopharmacol Biol Psychiatry.* 2013;**46**:64–9.
 - 22 Wang Q, He K, Li Z, Chen J, Li W, Wen Z, et al. The *CMYA5* gene confers risk for both schizophrenia and major depressive disorder in the Han Chinese population. *World J Biol Psychiatry.* 2014;**15**:553–60.
 - 23 Benson MA, Tinsley CL, Waite AJ, Carlisle FA, Sweet SMM, Ehler E, et al. Ryanodine receptors are part of the myospryn complex in cardiac muscle. *Sci Rep.* 2017;**7**:6312.
 - 24 Durham JT, Brand OM, Arnold M, Reynolds JG, Muthukumar L, Weiler H, et al. Myospryn is a direct transcriptional target for MEF2A that encodes a striated muscle, α -actinin-interacting, costamere-localized protein. *J Biol Chem.* 2006;**281**:6841–9.
 - 25 McGrath MJ, Cottle DL, Nguyen MA, Dyson JM, Coghill ID, Robinson PA, et al. Four and a half LIM protein 1 binds myosin-binding protein C and regulates myosin filament formation and sarcomere assembly. *J Biol Chem.* 2006;**281**:7666–83.
 - 26 Blair CM, Baillie GS. Reshaping cAMP nanodomains through targeted disruption of compartmentalised phosphodiesterase signalosomes. *Biochem Soc Trans.* 2019;**47**:1405–14.
 - 27 Nelson AR, Borland L, Allbritton NL, Sims CE. Myristoyl-based transport of peptides into living cells. *Biochemistry.* 2007;**46**:14771–81.
 - 28 Nakagami H, Kikuchi Y, Katsuya T, Morishita R, Akasaka H, Saitoh S, et al. Gene polymorphism of myospryn (cardiomyopathy-associated 5) is associated with left ventricular wall thickness in patients with hypertension. *Hypertens Res.* 2007;**30**:1239–46.
 - 29 Tran MK, Kurakula K, Koenis DS, de Vries CJ. Protein-protein interactions of the LIM-only protein FHL2 and functional implication of the interactions relevant in cardiovascular disease. *Biochim Biophys Acta.* 2016;**1863**:219–28.
 - 30 Yin X, Cuello F, Mayr U, Hao Z, Hornshaw M, Ehler E, et al. Proteomics analysis of the cardiac myofibrillar

- subproteome reveals dynamic alterations in phosphatase subunit distribution. *Mol Cell Proteomics*. 2010;**9**:497–509.
- 31 Lu F, Pu WT. The architecture and function of cardiac dyads. *Biophys Rev*. 2020;**12**:1007–17.
- 32 Chu PH, Ruiz-Lozano P, Zhou Q, Cai C, Chen J. Expression patterns of FHL/SLIM family members suggest important functional roles in skeletal muscle and cardiovascular system. *Mech Dev*. 2000;**95**:259–65.
- 33 Wixler V, Geerts D, Laplantine E, Westhoff D, Smyth N, Aumailley M, et al. The LIM-only protein DRAL/FHL2 binds to the cytoplasmic domain of several α and β integrin chains and is recruited to adhesion complexes. *J Biol Chem*. 2000;**275**:33669–78.
- 34 Samson T, Smyth N, Janetzky S, Wendler O, Muller JM, Schule R, et al. The LIM-only proteins FHL2 and FHL3 interact with α - and β -subunits of the muscle $\alpha7\beta1$ integrin receptor. *J Biol Chem*. 2004;**279**:28641–52.
- 35 Philippar U, Schrott G, Dieterich C, Muller JM, Galgoczy P, Engel FB, et al. The SRF target gene *Fhl2* antagonizes RhoA/MAL-dependent activation of SRF. *Mol Cell*. 2004;**16**:867–80.
- 36 Fimia GM, De Cesare D, Sassone-Corsi P. A family of LIM-only transcriptional coactivators: tissue-specific expression and selective activation of CREB and CREM. *Mol Cell Biol*. 2000;**20**:8613–22.
- 37 Hubbi ME, Gilkes DM, Baek JH, Semenza GL. Four-and-a-half LIM domain proteins inhibit transactivation by hypoxia-inducible factor 1. *J Biol Chem*. 2012;**287**:6139–49.
- 38 Reynolds JG, McCalmon SA, Tomczyk T, Naya FJ. Identification and mapping of protein kinase A binding sites in the costameric protein myospryn. *Biochim Biophys Acta*. 2007;**1773**:891–902.
- 39 Kouloumenta A, Mavroidis M, Capetanaki Y. Proper perinuclear localization of the TRIM-like protein myospryn requires its binding partner desmin. *J Biol Chem*. 2007;**282**:35211–21.
- 40 Sarparanta J, Blandin G, Charton K, Vihola A, Marchand S, Milic A, et al. Interactions with M-band titin and calpain 3 link myospryn (CMYA5) to tibial and limb-girdle muscular dystrophies. *J Biol Chem*. 2010;**285**:30304–15.
- 41 Feng W, Liu C, Spinozzi S, Wang L, Evans SM, Chen J. Identifying the cardiac dyad proteome *in vivo* by a BioID2 knock-in strategy. *Circulation*. 2020;**141**:940–2.
- 42 Rudolf R, Khan MM, Lustrino D, Labeit S, Kettelhut IC, Navegantes LC. Alterations of cAMP-dependent signaling in dystrophic skeletal muscle. *Front Physiol*. 2013;**4**:290.
- 43 Kielbasa OM, Reynolds JG, Wu CL, Snyder CM, Cho MY, Weiler H, et al. Myospryn is a calcineurin-interacting protein that negatively modulates slow-fiber-type transformation and skeletal muscle regeneration. *FASEB J*. 2011;**25**:2276–86.
- 44 Dema A, Perets E, Schulz MS, Deak VA, Klussmann E. Pharmacological targeting of AKAP-directed compartmentalized cAMP signalling. *Cell Signal*. 2015;**27**:2474–87.
- 45 Ewen EP, Snyder CM, Wilson M, Desjardins D, Naya FJ. The Mef2A transcription factor coordinately regulates a costamere gene program in cardiac muscle. *J Biol Chem*. 2011;**286**:29644–53.
- 46 Matulis CK, Mayo KE. The LIM domain protein FHL2 interacts with the NR5A family of nuclear receptors and CREB to activate the inhibin- α subunit gene in ovarian granulosa cells. *Mol Endocrinol*. 2012;**26**:1278–90.
- 47 Farrell E, Armstrong AE, Grimes AC, Naya FJ, de Lange WJ, Ralph JC. Transcriptome analysis of cardiac hypertrophic growth in *MYBPC3*-Null mice suggests early responders in hypertrophic remodeling. *Front Physiol*. 2018;**9**:1442.
- 48 Carrier L, Mearini G, Stathopoulou K, Cuello F. Cardiac myosin-binding protein C (MYBPC3) in cardiac pathophysiology. *Gene*. 2015;**573**:188–97.
- 49 Chang TH, Chen MC, Chang JP, Huang HD, Ho WC, Lin YS, et al. Exploring regulatory mechanisms of atrial myocyte hypertrophy of mitral regurgitation through gene expression profiling analysis: role of NFAT in cardiac hypertrophy. *PLoS One*. 2016;**11**:e0166791.
- 50 Zhang J, Huang X, Wang X, Gao Y, Liu L, Li Z, et al. Identification of potential crucial genes in atrial fibrillation: a bioinformatic analysis. *BMC Med Genomics*. 2020;**13**:104.
- 51 Port JD, Walker LA, Polk J, Nunley K, Buttrick PM, Sucharov CC. Temporal expression of miRNAs and mRNAs in a mouse model of myocardial infarction. *Physiol Genomics*. 2011;**43**:1087–95.
- 52 Knyazeva A, Krutikov A, Golovkin A, Mishanin A, Pavlov G, Smolina N, et al. Time- and ventricular-specific expression profiles of genes encoding Z-disk proteins in pressure overload model of left ventricular hypertrophy. *Front Genet*. 2018;**9**:684.
- 53 Frank R. The SPOT-synthesis technique. Synthetic peptide arrays on membrane supports—principles and applications. *J Immunol Methods*. 2002;**267**:13–26.
- 54 Bolger GB, Baillie GS, Li X, Lynch MJ, Herzyk P, Mohamed A, et al. Scanning peptide array analyses identify overlapping binding sites for the signalling scaffold proteins, β -arrestin and RACK1, in cAMP-specific phosphodiesterase PDE4D5. *Biochem J*. 2006;**398**:23–36.
- 55 Vignier N, Schlossarek S, Fraysse B, Mearini G, Kramer E, Pointu H, et al. Nonsense-mediated mRNA decay and ubiquitin-proteasome system regulate cardiac myosin-binding protein C mutant levels in cardiomyopathic mice. *Circ Res*. 2009;**105**:239–48.

- 1 56 Pohlmann L, Kroger I, Vignier N, Schlossarek S,
2 Kramer E, Coirault C, et al. Cardiac myosin-binding
3 protein C is required for complete relaxation in intact
4 myocytes. *Circ Res.* 2007;**101**:928–38.
- 5 57 Stathopoulou K, Schobesberger S, Bork NI, Sprenger
6 JU, Perera RK, Sotoud H, et al. Divergent off-target
7 effects of RSK N-terminal and C-terminal kinase
8 inhibitors in cardiac myocytes. *Cell Signal.*
9 2019;**63**:109362.
- 10 58 Eschenhagen T, Fink C, Remmers U, Scholz H,
11 Wattchow J, Weil J, et al. Three-dimensional
12 reconstitution of embryonic cardiomyocytes in a
13 collagen matrix: a new heart muscle model system.
14 *FASEB J.* 1997;**11**:683–94.
- 15 59 Diering S, Stathopoulou K, Goetz M, Rathjens L,
16 Harder S, Piasecki A, et al. Receptor-independent
17 modulation of cAMP-dependent protein kinase and
18 protein phosphatase signaling in cardiac myocytes
19 by oxidizing agents. *J Biol Chem.* 2020;**295**:15342–
20 65.
- 21 60 Schindelin J, Arganda-Carreras I, Frise E, Kaynig V,
22 Longair M, Pietzsch T, et al. Fiji: an open-source
23 platform for biological-image analysis. *Nat Methods.*
24 2012;**9**:676–82.
- 25
26
27
28
29
30
31
32
33
34
35
36
37
38
39
40
41
42
43
44
45
46
47
48
49
50
51
52
53